The Zagros Folded Belt (Fars, Iran): Consraints from Topography and Critical Wedge Modelling

Frédéric Mouthereau, Olivier Lacombe, Bertrand Meyer

Geophys. J. Int. (2006) **165,** 336–356 doi: 10.1111/j.1365-246X.2006.02855.x

The Zagros folded belt (Fars, Iran): constraints from topography and critical wedge modelling

F. Mouthereau, O. Lacombe and B. Meyer

Lab. Tectonique, UMR7072, *UPMC, France,* 75252 *Paris Cedex* 05. *E-mail: frederic.mouthereau@lgs.jussieu.fr*

Accepted 2005 October 26. Received 2005 August 13; in original form 2005 April 6

SUMMARY

The Late Miocene tectonics of the Zagros folded belt (Fars province) has for long been related solely to folding of the cover controlled by a ductile décollement between basement and the sedimentary cover. However, geological constraints, topography analysis and seismotectonic studies reveal that basement thrusting may produce locally significant deformation in the cover. To determine how the deep-seated deformation in the basement may contribute to the overall topography we first examine the filtered large and short wavelengths of the topography. We find that the short-wavelength component of the topography (20–25 km), including the Zagros folds, is superimposed on the differential uplift at the regional scale. In other words, the regional base level of folded marker horizons remains parallel to the regional topography of interest. Modelling reveals that the salt-based wedge model, alone, is not able to reproduce the large-wavelength component of the topography of the Zagros Folded Belt. This reveals that when a thick (relatively to its overburden) layer of salt forms the basal décollement it is generally too weak and cannot support the growth of significant topography. We then test an alternative thick-skinned crustal wedge model involving the crust of the Arabian margin, which is decoupled above a viscous lower crust. This model satisfactorily reproduces the observed topography and is consistent with present-day basement thrusting, topography analyses and geological constraints. We conclude that basement-involved thickening and shortening is mechanically required to produce the shape of the Zagros Folded Belt since at least 10 Ma. Finally, the involvement of the basement provides mechanical and kinematic constraints that should be accounted for cross-sections balancing and further assessing the evolution of Zagros at crustal or lithospheric scales.

Key words: mountain building, topography, Zagros.

1 INTRODUCTION

The Zagros fold-thrust belt (Fig. 1) results from the continent–continent collision between the Arabian margin and the Eurasian plate following the closure of the Neo-Tethys ocean during the Tertiary (Stocklin 1968; Falcon 1974). Despite some ongoing controversies about the timing of the onset of the collision (Hessami *et al.* 2001), there is little doubt that the main episode of cover shortening in the Zagros folded belt occurred since about 10 Ma as suggested by the youngest folded strata of the Agha Jari red marls (Fig. 2). Shortening of about 70 km derived from balanced sections across the Zagros folded belt (McQuarrie 2004) yields shortening rates of 7 km Ma^{-1} consistent with the present-day rates of 0.7 cm yr^{-1} based on GPS studies (Vernant *et al.* 2004). A major unconformity between the Agha Jari formation and the Bakhtyari conglomerates (Fig. 2) indicates that cover shortening decreased or ceased 5 Ma ago. During or since the deposition of the Bakhtyari Formation, the Zagros fold belt underwent a regional uplift whose origin still remains enigmatic.

The Fars province is located to the southeast of the Zagros fold belt (Fig. 1). The deformation in this part of the belt is characterized by periodic folding with axial lengths sometimes greater than 200 km (Fig. 3). This fold geometry is outlined by the limestones beds of the Asmari Formation, which is one of the main oil reservoirs in the Zagros. The folded Meso-Cenozoic sedimentary cover is about 10 km thick and overlies a basal layer of salt represented by the Cambrian Hormuz Formation, which is up to 1–2 km thick (Fig. 2). This salt-bearing formation is known to be particularly mobile as it forms one of the largest province of salt diapirs worldwide (Jackson *et al.* 1990; Talbot & Alavi 1996). The Fars domain of the ZSFB is limited to the west by a main structural, topographic and palaeogeographic boundary: the Kazerun fault (KzF)(Motiei 1993) (Fig 3). It is a major N–S trending active right-lateral strike-slip fault inherited from the Late Proterozoic fault system of the Pan-African basement (Talbot & Alavi 1996). The reactivation of such a set of inherited faulted basement blocks probably controlled salt diapirism in the Persian Gulf area (Egdell 1996).

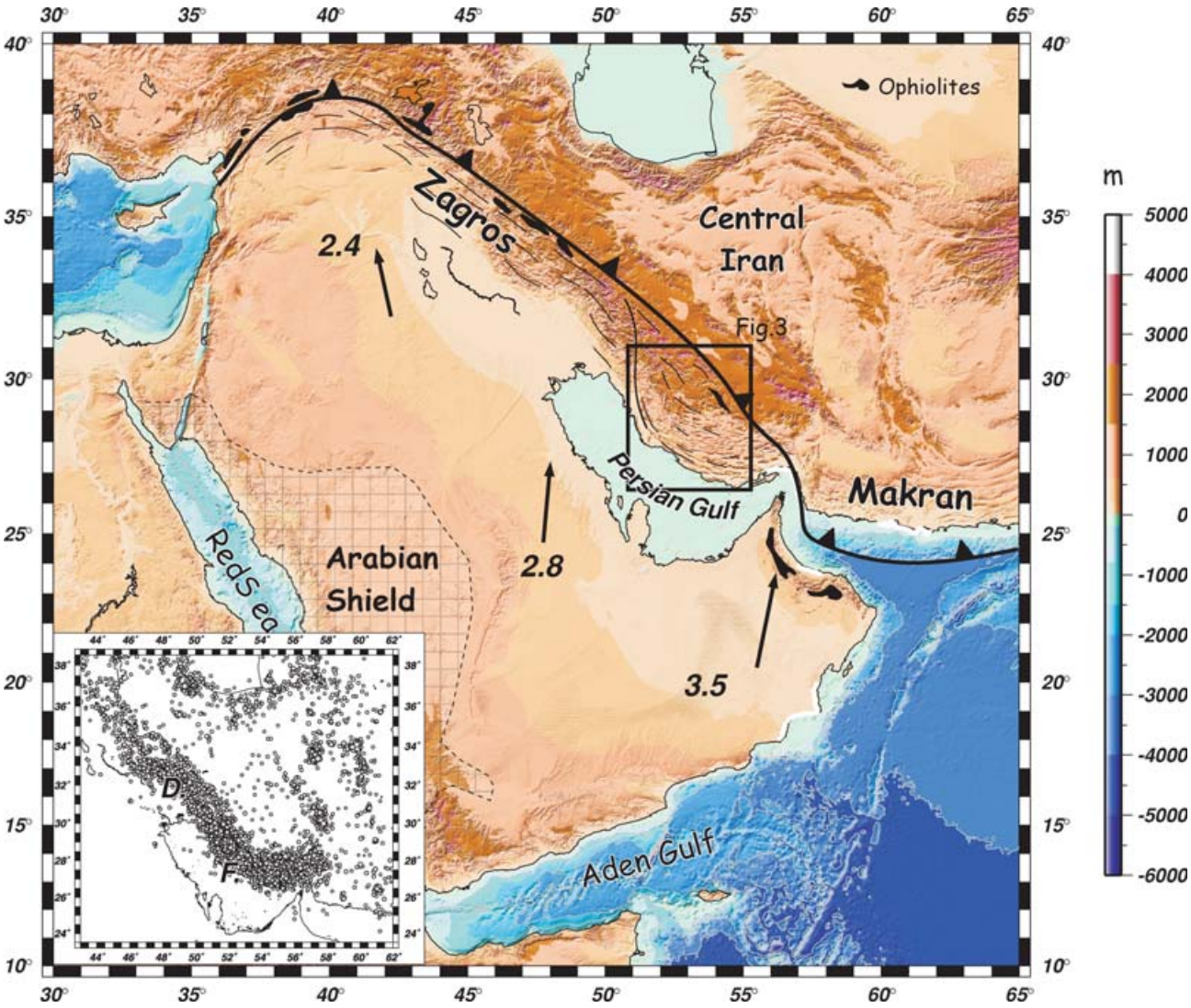

Figure 1. Simplified geodynamic framework of the Zagros fold belt. Black arrows show the present-day convergence between the Arabian plate and stable Eurasia deduced from current global plate motion Nuvel 1A (De Mets *et al.* 1994). The grey rectangle indicates the study area of the Fars province. The inset shows the distribution of earthquakes ($2.4 < m_b < 7.4$) in the Zagros collision belt with focal depths lower than 35 km issued from ISC and CMT catalogues (1965–2003). It shows that the Fars domain at the front of the MZT highlighted by seismicity, accommodates part of the Arabia–Eurasia convergence. Many of the earthquakes in the Zagros correspond to events occurring in the basement. Inset: D. for Dezful and F. for Fars areas.

In an attempt to explain the geometry and kinematics of folding in such a salt-based fold belt, Davis & Engelder (1985) noticed that applying the theory of frictional wedges to the Zagros folded belt is not straightforward because of the salt-based plastic décollement. They consequently adapted the theory of thrust wedges based on a plastic pressure-independent behaviour of the décollement level. In parallel, sand-box experiments involving silicone putty as an analogue to viscous properties of salt décollement provided important results on the way the spatial distribution of salt controls the shape of the folded belt and the sequence of deformation (Jackson *et al.* 1990; Weijermars *et al.* 1993; Costa & Vendeville 2002; Bahroudi & Koyi 2003). In the Fars province, the low topography and the lack of clear fold vergence were considered to be characteristic of a thin-skinned fold-thrust belt controlled by the extreme weakness of the salt at its base (Davis & Engelder 1985). Davis & Engelder (1985) predict that such salt-based wedges have very narrow tapers $<1^\circ$ and are characterized by the absence of significant topography Jaumé & Lillie (1988), applying the same analytical approach to the case of the Potwar Plateau-Salt Ranges, showed that an increase in the décollement dip β, for example, due to plate flexure, would theoretically lead to negative or essentially flat topography. Recently, Ford (2004), based on natural examples as well as analogue and numerical modelling, suggested that the final topography in salt-based wedges may be independent of the décollement dip that is controlled by plate flexure. This is supported by recent sandbox models of brittle–ductile wedges (Smit *et al.* 2003) as changing β has little effect on α. These recent studies reveal that the mechanisms of deformation within such fold belts are not fully explained by the current critical wedges theory. Thus, we would like to test in the light of the recent data on the Zagros structure and constraints on the rheology of salt if such theory can produce the observed topography.

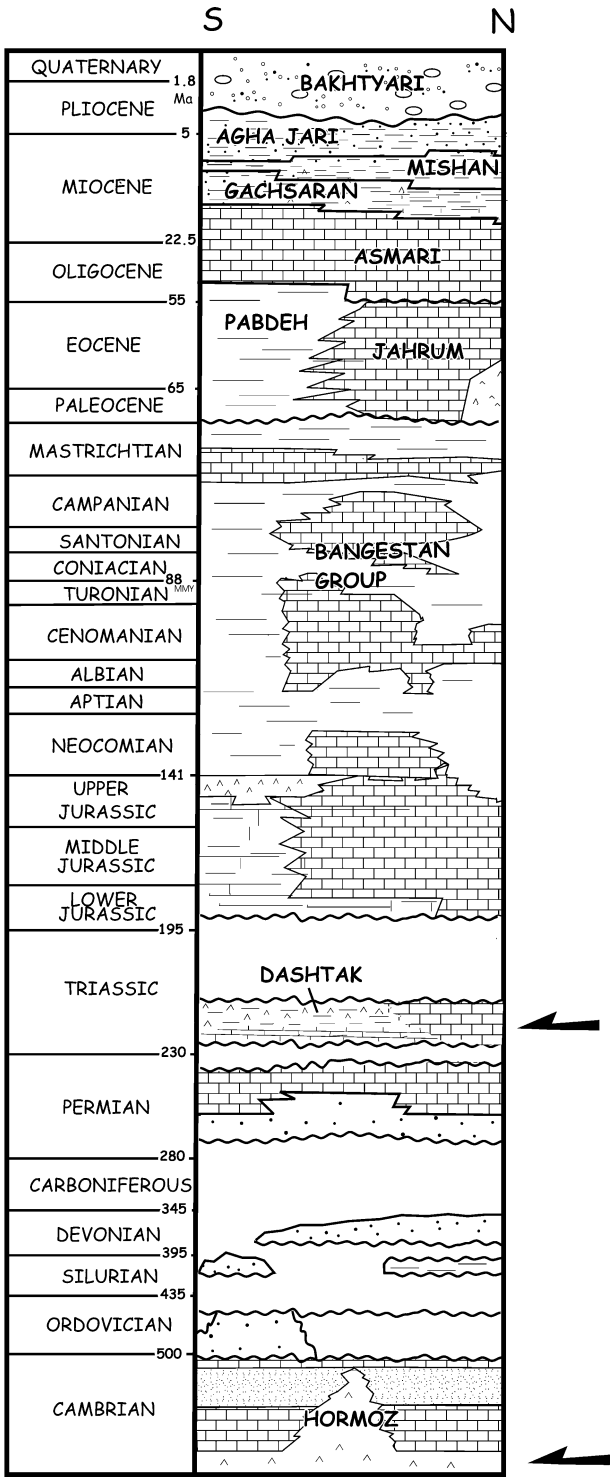

Figure 2. Simplified chronostratigraphic chart and lithologies encountered in the Fars fold belt after (Motiei 1993). Black arrows indicate the position of weak evaporitic layers in the sedimentary pile that potentially act as a décollement level. The main décollement lies within the Eo-Cambrian salts of the Hormuz formations at the base of the Meso-Cenozoic sedimentary cover. The Dashtak formation can also act as décollement but essentially in the Coastal Fars.

Seismotectonic studies over the last 20 yr have provided evidence that the Precambrian basement is shortening and thickening (Jackson 1980; Berberian & King 1981; Ni & Barazangi 1986; Berberian 1995). For instance, Jackson (1980) first observed that dips of nodal planes are typically in the range 30°–60°, suggesting that shortening in the basement results from the inversion of normal faults formed during the Palaeozoic–Mesozoic Tethyan rifting of the Arabian margin. Because the position of earthquake hypocentres are not well constrained, basement deformation has not been considered by some authors as critical for understanding the topography, geometry and kinematics of the Fars folded belt (McQuarrie 2004). On the other hand, recent seismological studies based on the relocation of earthquakes or new accurate estimates of the depths of earthquakes from local seismological network have confirmed that many of the hypocentres are effectively located below the sedimentary cover (Talebian & Jackson 2004; Tatar *et al.* 2004). This has renewed our interest in basement involvement and its possible control on the geometry and kinematics of the Zagros fold belt.

The idea of shortening in the Precambrian basement below the salt décollement is not recent. For instance, one can refer to a work by Comby *et al.* (1977) republished in Egdell (1996) who proposed a cross-section of the Fars in which the basement comprises two large thrust slabs above which the sedimentary cover is folded independently above the mobile Hormuz Salt Formation. Also, geophysical modelling and interpretation of Bouguer gravity data have been interpreted as showing a link between the deflection of the Arabian plate below the Zagros and the response of crustal thickening at different levels, within the Hormuz salts and the basement to about 25 km above a ductile lower crust (Snyder & Barazangi 1986).

More recently, balanced cross-sections (Blanc *et al.* 2003; Sherkati & Letouzey 2004) suggest that basement thrusting is required to explain the present-day topography and the difference in elevation of the Palaeozoic and Mesozoic Formations. Balanced cross-sections in the southeastern Fars (Molinaro *et al.* 2004) also suggest that the Precambrian basement is involved in tectonic thickening. In an attempt to propose the timing of basement involvement deformation, a recent model (Molinaro *et al.* 2005) suggests that the development of the thick-skinned folded belt became prominent 5 Ma ago following an initial episode of thin-skinned folding in the Zagros. These numerous hypotheses need to be tested in the light of mechanical modelling.

In this paper, we test and validate mechanically different hypotheses proposed for the present and long-term kinematics of the Zagros folded belt:

(1) a shallow wedge of sedimentary cover detached above a salt-based décollement;

(2) a thick wedge of upper crystalline basement decoupled above a ductile lower crust.

The input data are topography, seismicity and geological data. The topography in such an active folded belt is believed to be a direct response to the mechanics of the wedge. The topographic data are analysed in order to identify large wavelengths that are related to distributed deformation across the Fars and shorter wavelengths reflecting the topographic signature of folding. Then we examine whether the thin-skinned or thick-skinned style of deformation better reproduces the observed topographic patterns. We adopt a critical wedge approach (Davis *et al.* 1983; Dahlen 1990) to test both hypotheses. Our results suggest that if a tectonic wedge is required to reproduce the observed pattern of seismicity, the geological data and the first-order topography of the Zagros folded belt, it should involve deformation of the crystalline basement.

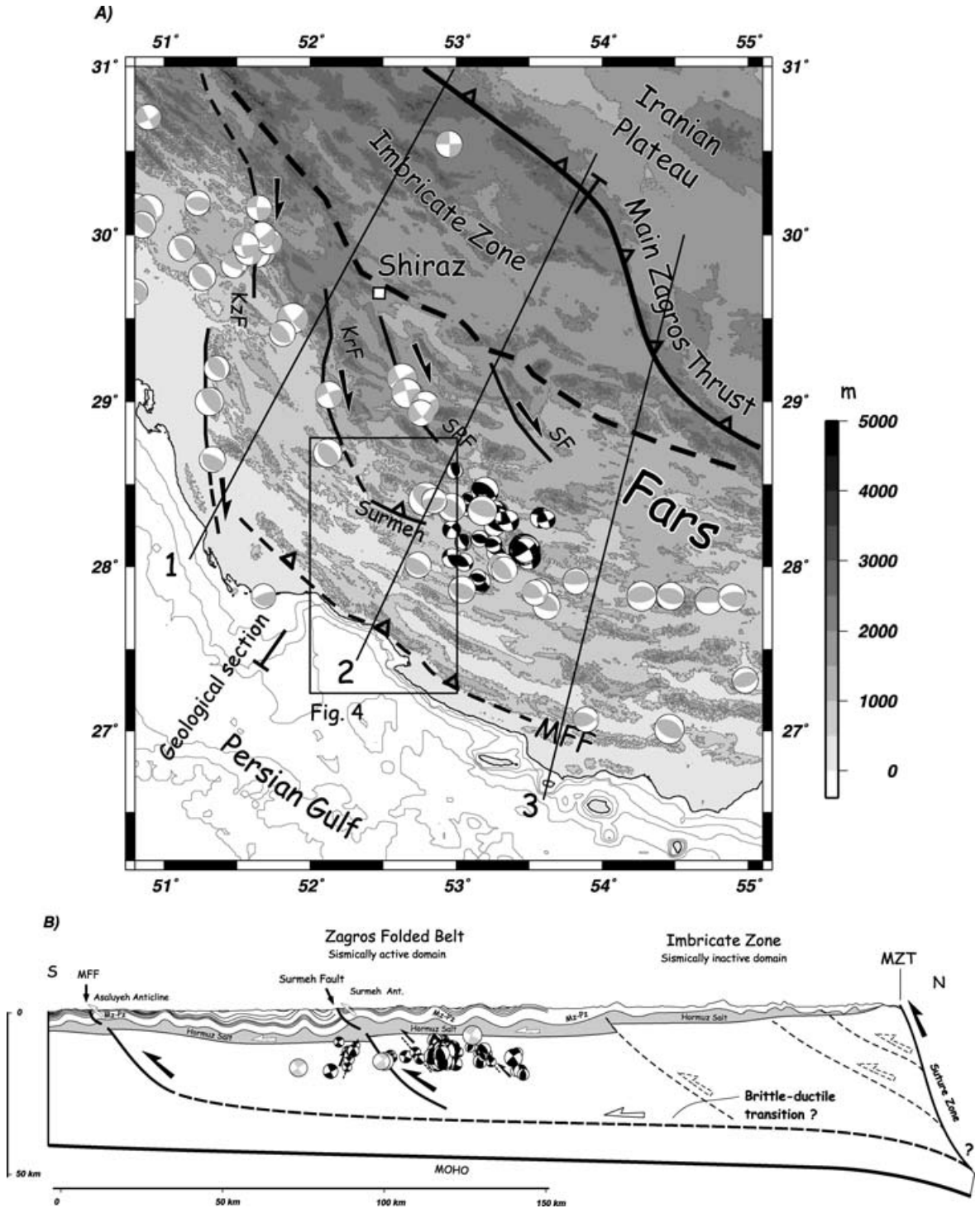

Figure 3. (a) Topography (SRTM data) and main structural features and (b) a simplified geological section across the Fars. Sections numbered 1, 2 and 3 correspond to the topographic profiles studied in Fig. 8. The folded sedimentary cover is decoupled from the basement above Hormuz Salt Formation. The present-day and long-term deformation within the basement is attested along the MFF and the Surmeh Fault in agreement with the position of the main basement faults presented by several works (Berberian 1995; Talebian & Jackson 2004). Focal mechanisms reveal that the basement is deforming and thickening along distributed faults probably inherited from Permo-Triassic rifting. White dashed arrows are postulated high-angle reverse faults below the Imbricate Zone, which are not associated with seismic activity. Fault plane solutions ($4.6 < M_w < 6.7$) from (Talebian & Jackson 2004) are shown with focal spheres in light grey. Focal mechanisms of small earthquakes ($1.7 < M_L < 4.1$) determined from local network (Tatar *et al.* 2004) are shown with black focal spheres. The size of focal spheres is proportional to the magnitudes of earthquakes. MFF: Mountain Front Fault; MZT : Main Zagros Thrust; KzF: Kazerun Fault; KrF: Karebass Fault; SPF: Sabz-Pushan Fault; SF: Sarvestan Fault and Pz–Mz: Palaeozoic–Mesozoic sedimentary cover. All these faults are basement faults and affect the sedimentary cover. The MFF that is depicted by a dashed line is probably a buried fault.

2 BASEMENT THRUSTING IN THE FARS

2.1 Geological evidence indicating age of activity on the Mountain Front Fault (MFF) and Surmeh fault

The Fars province is an arcuate folded area of 200 km wide showing little evidence of major thrust faulting at the surface (Fig. 3). The folded sedimentary cover is composed of a 10–12-km-thick pile of Palaeozoic and Mesozoic strata (Falcon 1974; Stocklin 1974; Colman-Sadd 1978). The lithology of rocks enables a division into a lower mobile group in the Eo-Cambrian salts of the Hormuz formation and an upper competent group represented by the thick Mesozoic–Cenozoic strata (Fig. 2). This differs from the Dezful province where the Miocene salts of the Gashsaran Formation form an upper mobile group (O'Brien 1957). More specifically, the Dashtak Formation of Triassic age comprised of evaporitic beds and may potentially act as an intermediate décollement within the sedimentary cover in the NW of the Zagros basin and Coastal Fars.

The famous 'whaleback' shape of folds outlines the periodic and monoharmonic succession of folds across the Fars (Fig. 3). Despite the apparent continuity of structures, morphology and surface geology, two relatively significant topographic and structural features can be recognized: the MFF and the Surmeh Fault distant by 100 km (Figs 3 and 4). In the following, we have used the nomenclature defined by Berberian (1995) for major basement faults. The MFF (Berberian 1995) is also called the Mountain Front Flexure by McQuarrie (2004) or the Zagros Frontal Fault by Sepher & Cosgrove (2004). The Surmeh Fault is called the MFF by Sepher & Cosgrove (2004).

The topographic step outlined by the MFF is located at the front of the Asaluyeh Anticline, a 200-km-long, 1500-m-high, coastal fold that brings the Mesozoic strata up to the surface. Topographic sections across the anticline show that the regional base level is about 700 m higher to the north (Figs 4 and 5a). In the centre of the Fars folded belt, a second topographic offset of 500 m occurs across the faulted Surmeh Anticline (Fig. 5b), one of the few folds of the ZFB where Palaeozoic strata are exposed.

Taking into account the regional importance of the topographic steps, and considering a constant sedimentary cover thickness across both anticlines, the top of the basement should be vertically offset by nearly similar amounts. The contribution of viscous upward flow and salt pinch-out of the Cambrian salt (McQuarrie 2004) to the total elevation of the Asaluyeh anticline is difficult to quantify but this mechanism cannot account for the large-scale topographic step. If we assume a maximum dip of 60° for these basement faults consistent with seismicity (e.g. Jackson 1980) the related slip should be about 810 m and 570 m along the MFF and the Surmeh fault, respectively.

2.2 Localized basement faulting and seismicity: evidence from the Mountain Front and the Surmeh Faults

The depth distribution of crustal earthquakes suggests that many of the hypocentres are deeper than 10 km, that is, located in the Precambrian basement (Maggi *et al.* 2000). If this is reliable, the distribution of epicentres issued from ISC and CMT catalogues indicates pervasive seismogenic deformation in the basement (Figs 1 and 3). A local seismic network has provided the record of 416 small earthquakes ($1.7 < M < 4.1$) in the region of the Qir earthquake (Tatar *et al*. 2004). The depth location of the hypocentres first confirms that active faulting occurs below 11 km in the basement. 73 focal mechanisms were derived from this study. These mechanisms confirm earlier work (Jackson 1980) in that they highlight active high-angle reverse faulting in the basement. These basement thrusts result from the reactivation of earlier normal faults inherited from Tethyan rifting.

The present-day activity of the MFF and Surmeh faults is demonstrated by extensive seismotectonic analyses performed by Berberian (1995). The southern limb of the Surmeh Anticline is bounded by a major active basement fault: the so-called Surmeh Fault. This major thrust fault is connected with the Karebass fault (KrF), a major right-lateral transverse fault rooted into the basement. Recent destructive earthquakes like the Qir (1972, $M_S = 6.9$) and the Lar (1966, $M_S = 6.2$) earthquakes (Berberian 1995) are located a few kilometres to the east of the Surmeh Anticline. Furthermore, the present-day kinematics and geometry is revealed by some focal mechanisms in the Lar area (Fig. 3). For the MFF, Berberian (1995) suggested that the location of the Asaluyeh anticline coincides with the trace of a major seismic trend along which large-to-moderate earthquakes occur on buried high-angle basement reverse fault segments. Thus it is likely that the present-day topographic step of 700 m mentioned before is related to the cumulative displacement along this deep-seated reverse fault.

2.3 Long-lived basement thrusting: constraints from Miocene basin geometry

The subsidence history of the Precambrian basement in the Zagros basin has received little attention in the literature. However, in an attempt to constrain this history, overall subsidence curves in the Zagros basin have suggested that the collision-related flexure occurred about 30–20 Ma ago, during or soon after the deposition of the Asmari Limestones (Sherkati & Letouzey 2004). It follows that the later clastic deposits of the Fars Group (Gashsaran, Mishan and Agha Jari Formations from bottom to top) are synrorogenic strata deposited in the Neogene flexural basin of the Zagros.

Isopachs of the Mishan Formation (Motiei 1993) provide constraints on the palaeotopography at the time of deposition, that is, at Middle to Upper Miocene age (∼16–11 Ma), in the Zagros basin (Fig. 6). At the scale of the basin, these isopachs reveal that the thickness of the Mishan formation increases from 0 to 300 m at the Persian Gulf to 600 or 900 m towards the north. Then further to the north the thickness of strata decreases again to only 300 m at the boundary with the Imbricate Zone. This defines a central 70 km wide depocentre in the northwestern part of the Mishan basin that progressively widens towards the south to about 150–200 km. Near the Imbricate Zone, a relatively uplifted domain bounding the basin to the north may represent part of the uplifted Zagros fold belt at that time. In the northern part of the Mishan basin, near the KrF, the thickness of the Mishan Formation locally reaches more than 1200 m. Within a few tens of kilometres southwards the thickness decreases to less than 300 m thus defining a local uplift. A set of uplifted domains can be recognized that are bounded to the south, with respect to the central depocentre, by the Surmeh Fault. These data suggest that the filling of the Mishan basin occurred coevally with folding and/or thrusting in the vicinity of the Surmeh Fault. Isopachs further reveal that the area to the south of the Surmeh fault was affected by significant subsidence. The contrast with the relative uplift observed in the hanging wall of the Surmeh Fault suggests that the Surmeh Fault was active at that time and caused flexure of the southernmost Fars by thrust loading.

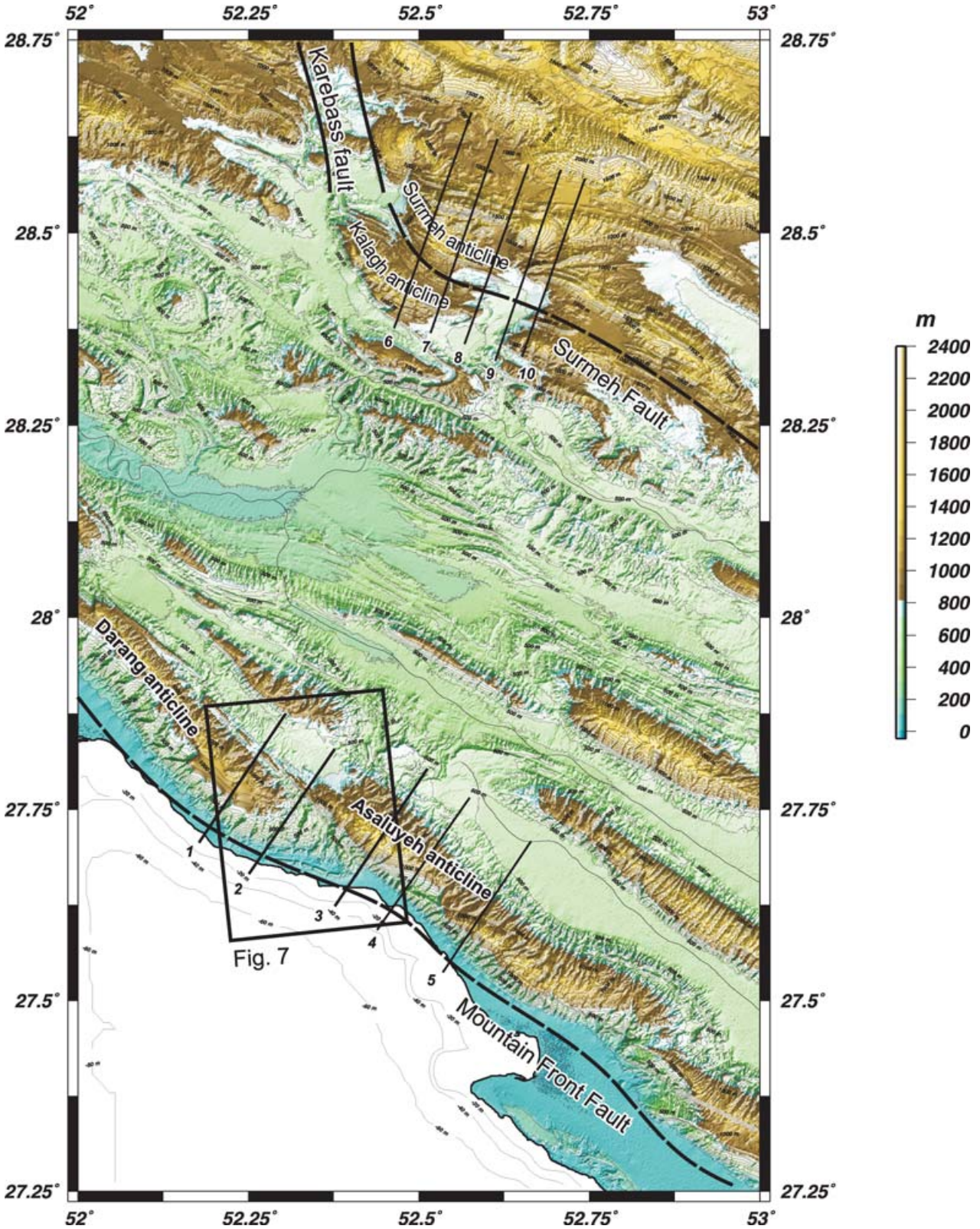

Figure 4. Topographic map of the Central Fars (90 m resolution STRM data). The uplift associated with the MFF and the Surmeh Fault is clearly outlined. The structural and kinematic relationships between the basement strike-slip fault of Karebass and the Surmeh Fault are also clearly shown. Subsurface data show that the central depression corresponds to a depocentre of the Mishan Formation (Middle Miocene). The quadrangle close to the MFF corresponds to the location of Fig. 7(a). For cross-sections 1–5 and 6–11 see Figs 5(a) and (b), respectively.

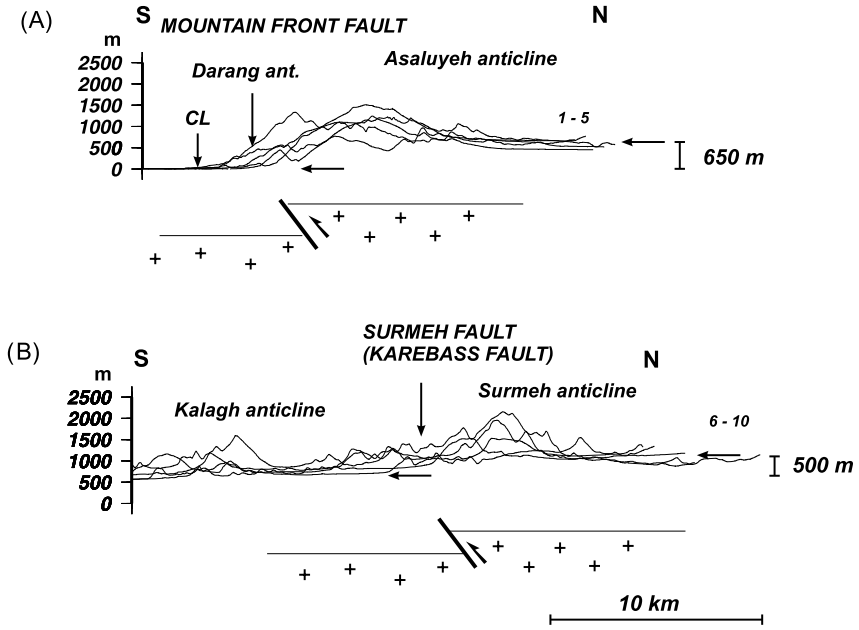

Figure 5. Local topographic sections across: a) the MFF (Asaluyeh Anticline) and b) the Surmeh Fault (see location in Fig. 4). Numbers on the left side of the drawing correspond to number of the sections located in Fig. 4. For both the MFF and the Surmeh Fault, a major topographic step is observed. Independent geological data (see Figs 6–8) and seismotectonic studies (Berberian 1995) suggest that this step is related to the uplift on buried basement reverse faults.

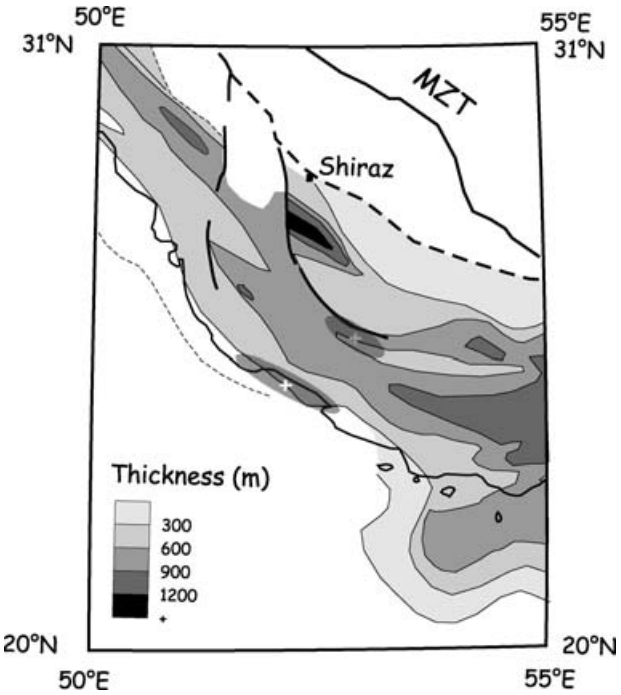

Figure 6. Isopach map of the Mishan Formation (16–11 Ma) from (Motiei 1993). The central depocentre is bounded by two moderate-scale uplifted areas (plus sign). These highs coincide with the position of the Surmeh Fault to the north and the buried MFF to the south.

At the southern border of the Mishan basin, field investigations close to the MFF in the Darang Anticline reveal that the Mishan Formation is present (Fig. 7). A more detailed study in the forelimb of the Asaluyeh anticline suggests that the Gashsaran Formation and the base of the Mishan Formation are missing above the Asmari Limestones (Fig. 7). This remarkable stratigraphic hiatus suggests that the southern part of the Zagros basin was uplifted above sea level and folded during the Upper Miocene. This field observation indicates that folding was active early and far to the south of the Fars. Note that the location of the unconformity is located surprisingly close to the vicinity of the current position of the MFF. Unfortunately, these data are not sufficient to unequivocally demonstrate basement involvement. We note, however, that the cover folding might be directly or indirectly related to the activity of the buried MFF at that time. Further studies are required to solve this point. In terms of the sequence of deformation, if the activity of cover folding or the activity of the MFF during Middle Miocene is confirmed, this would suggest that deformation had already reached the current position of the MFF as early as 16–11 Ma. This is not consistent with a progressive migration of the deformation towards the foreland during the Tertiary.

3 WAVELENGTH ANALYSIS OF THE TOPOGRAPHY: CONSTRAINTS ON STRUCTURAL STYLES

3.1 Introduction and scope

The style of deformation in the Fars area is characterized by symmetrical regularly spaced folds of similar amplitude (Figs 3 and 4) and the noticeable lack of macroscopic reverse faults except where basement faults have been recognized. The nearly sinusoidal shape of folding allows the topography to be considered as a periodic signal whose wavelength is related to shortening at a given crustal level. This local signal is superimposed on a much larger scale signal that results from distributed shortening at the same crustal level or deeper. For instance, if no differential topographic elevation is found across a set of folds of wavelength λ

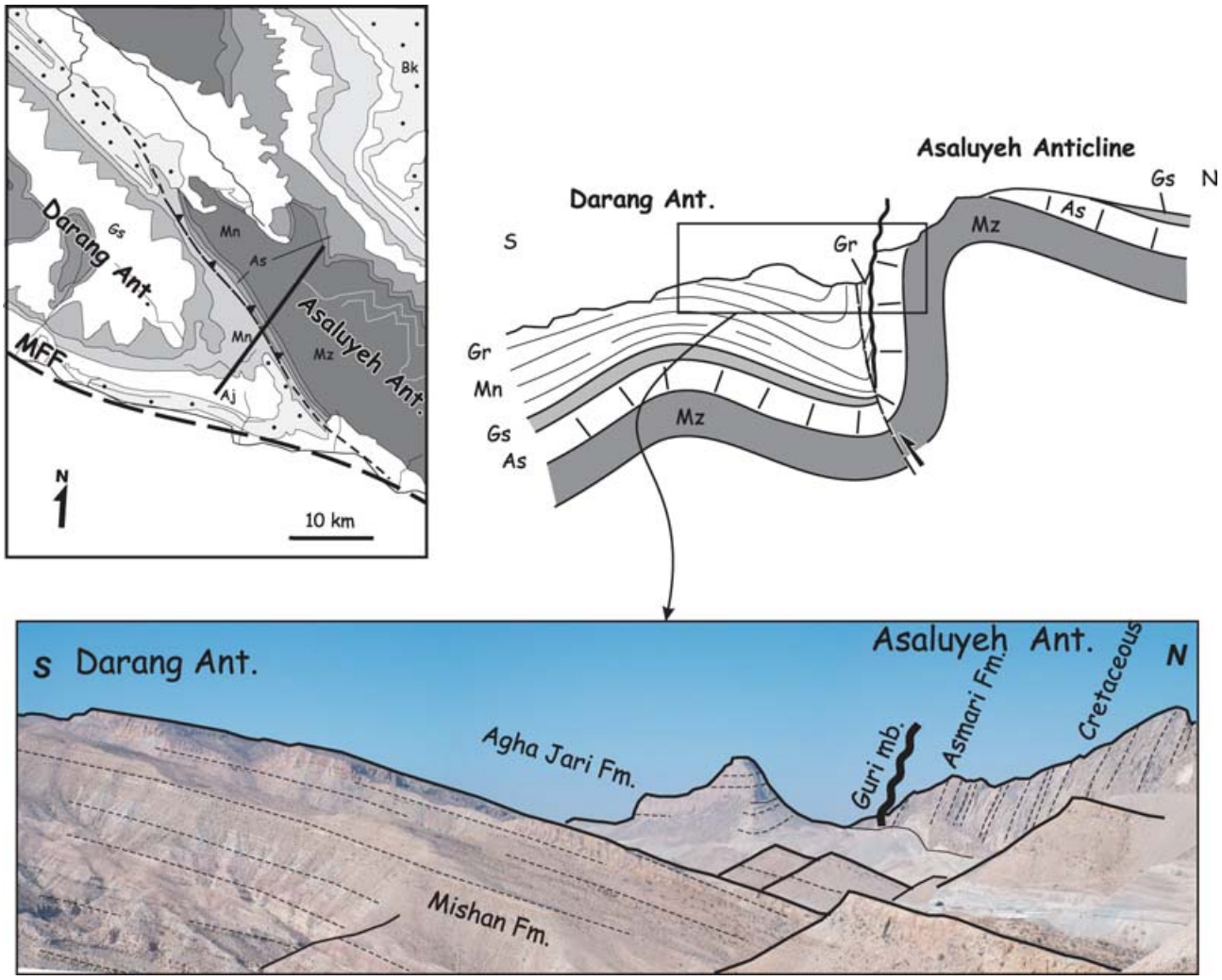

Figure 7. Geological section across the Darang and Asaluyeh Anticlines. A hiatus in the Mishan Formation (16–11 Ma) and the older Gashsaran Formation is observed above the Asmari Limestones. The local reverse fault that cuts the Tertiary sediments in the hinge of the Asaluyeh Anticline is probably related to folds kinematics and indirectly related to the kinematics of the buried MFF. Gr: Guri Member (upper part of the Mishan formation); Mn: Mishan Formation; Gs: Gashsaran Formation; As: Asmari Formation and Mz: undifferenciated Mesozoic strata.

the residual topographic slope observed after the removal of this wavelength should be zero. Otherwise, the residual topography observed may be caused by distributed shortening in the cover or in the basement. We will examine the different possibilities in a next section.

Our approach consists of applying high-pass and low-pass filters performed using a 2-D fast Fourier transform algorithm provided by the Generic Mapping Tools software (Wessel & Smith 1998) to the topographic data in order to identify and study the different wavelengths of the topography. To test whether the topography results from superimposed signatures of deformation at different crustal levels we examine which wavelengths reflect the regional and local topography and how the different levels of crustal deformation interact together. As we neglect the contribution of mantle dynamics to the topography observed such an approach requires that the studied topography be related simply to crustal deformation.

3.2 Short and large wavelength components of the topography

(a) Wavelengths $\lambda < 40$ km: 'whaleback' geometry of Zagros folding

Over the 200 km width of the Zagros folded belt, between the Persian Gulf and the MZT, the distance between two successive folds (i.e. the wavelength of folding), is constant $\lambda = 20$–25 km (Figs 3 and 4). The shape of folds through the Zagros belt is outlined by the geometry of the Asmari carbonates. This suggests that folding is accommodated homogeneously and above a single basal décollement level in the sedimentary cover. Similar conclusions are obtained by the balanced cross-sections in which folding is interpreted as the result of loosely spaced thrusting accommodating little displacement and rooting at depth in the Cambrian décollement (McQuarrie 2004; Sherkati 2004).

We first extract the local topographic signal from the overall data (3-arc sec SRTM topography with resolution of 90 m) by filtering wavelengths shorter than 40 km (twice the wavelength of the folds). The 2-D along-strike variations are studied along three topographic sections (Figs 8a, b and c).

The short wavelength topography coincides with the 'whaleback' folds (Fig. 8a). At such short wavelengths the largest amplitude amounts to 1000 m, close to major active basement fault zones. For instance, the sharp increase of the elevation near the Gulf corresponds to the position of the MFF (Sections 2 and 3). Northwards, some noticeable topographic highs (500–1000 m) are correlated with the position of active transpressive strike-slip faults such as KzF, KrF, Sabz-Pushan (SPF) or Sarvestan (SF) faults. Section 3 is characterized by small amplitudes of 500 m maximum, expected close to the Imbricate Zone and the Main Zagros Thrust (MZT).

(b) Wavelengths $\lambda > 40$ km: the Zagros thrust wedge

Now, short wavelengths are removed from the total topographic signal using a low-pass filter (Fig. 8a). The residual topography contains only wavelengths larger than 40 km (Fig. 8b). The results are shown along three profiles (Fig. 8c).

The short-wavelength component of the topography is essentially superimposed on the differential uplift at the regional scale. This outlines that the intensity of deformation associated with folding is remarkably homogeneous in amplitudes and wavelengths defining a quasi-perfect sinusoidal topographic signal across the region. In other words, the regional base level of folded marker horizons remains constant and parallel to the regional topography of interest.

Some large-scale trends are clear. There is an overall increase of elevation from 0 to 2500 m across the Zagros folded belt (Fig. 8c). One can also observe the decrease of the elevation from the NW of the belt to the SE. This regional trend appears closely related to topographic elevation in the vicinity of active transpressive strike-slip faults. This is particularly clear for KrF, SPF or KzF. A more refined analysis, not shown for brevity, indicates that the MFF, KzF and KrF are associated with intermediate wavelengths comprised between 40 and 100 km and steps of about 600 m for the MFF and more than 1200 m for the Karebass–Kazerun Fault Zone. The larger wavelengths ($\lambda > 100$ km) correspond to the topography of interest related to differential regional uplift. It is interesting to note that after the removal of the wavelengths associated with the basement faults such as the KzF/MFF and KrF/Surmeh Fault a regional topographic slope remains.

The major role played by the transpressive basement faults in the location of topographic steps suggests that they have accommodated significant vertical offsets. The observation of reverse focal mechanisms in the vicinity of the faults (KrF and KzF) accounts for their current reverse motion at least along some segments (Fig. 3a). These N–S trending faults have been reactivated many times since the Precambrian. Isopach maps of the Jurassic and Cretaceous reveal that the KzF was activated as transfer faults during the Tethyan tectonics (Sepher & Cosgrove 2004). A comparison of the thickness of strata accumulated during the Upper Cretaceous/Early Tertiary (Motiei 1993; Sepher & Cosgrove 2004) also indicate that the KzF was a major faulted boundary that accommodated the differential vertical displacement between the Dezful area in which 4–5 km of Pliocene strata were deposited and the Fars which remains a relative uplifted domain. Moreover, the kinematics of the KzF and KrF is today closely related to the thrust movement along the MFF and the Surmeh Fault, respectively.

4 STRUCTURAL STYLES AND TECTONIC WEDGING

In this part, we examine qualitatively, on the basis of mechanical, lithological and geometric assumptions, which type of structural style can best explain the regional-scale topographic slope.

Since the work of Chapple (1978) and further development by Davis *et al.* (1983) it is accepted that the regional topography in most foreland fold-thrust belts results from the tectonic wedging of crustal rocks. The wedge shape of fold-thrust belts is induced by the frictional resistance above a basal décollement, which is balanced by gravitational forces arising from the topography. This model is theoretically scale independent so the basal décollement level can be located within the sedimentary cover or deeper in the mechanically weakened lower crust.

Because of the number of structural possibilities to fit the regional topography, we examine here three end-members (Fig. 9). The first structural model assumes that the regional topographic elevation may result from the tectonic thickening at the base of the folded sedimentary cover in response to ductile thickening within the evaporites of the Hormuz Formation (Fig. 9a). The second case assumes that the observed topography results from the tectonic thickening due to folding and thrusting within the brittle cover that is detached above the Hormuz salts (Fig. 9b). Finally, the third and last hypothesis accounts for a regional topography that is related to the thickening of the basement along steep deep-seated reverse faults (Fig. 9c). For all models we assume that changes in the pre-orogenic sedimentary cover have negligible effects.

4.1 Ductile thickening in the Hormuz Salts

In this first case, we assume that the sedimentary cover is deforming by periodic folding and small-scale faulting that are superimposed on the regional topography. In order to reproduce the differential regional uplift of interest it is necessary to tectonically thicken the Cambrian salts by almost ~2–2.5 km, which is the maximum topographic elevation (Fig. 9a). Considering that the uplift was achieved mostly after the deposition of the Agha Jari formation ~5–10 Ma ago (see Introduction), the corresponding uplift rate should be at least ~0.2–0.5 mm yr^{-1}.

For each increment of deformation, the body forces arising from the overburden tends to reduce topography. The rate at which the 2–2.5 km elevation should diminish can be approached by assuming that salt will flow as a Newtonian viscous fluid. The lateral pressure gradient created by the differences in altitude between the elevated regions of the inner folded belt and the lower adjacent regions will produce a forelandward flow of salt. The rate of the viscous flow V in the centre of a channel of salt of height $h = 2$ km (maximum thickness of the undeformed salts) can be calculated using a Poiseuille flow formulation (Turcotte & Schubert 1982):

$V = \frac{1}{2\eta_{\text{salt}}} \cdot \frac{dP}{dL} \cdot (\frac{h^2}{4})$, where $\frac{dP}{dL} = \frac{\rho_{\text{salt}} g \Delta h}{L}$ is the pressure gradient; ρ_{salt} is the density of salt 2200 kg m^{-3}, which is the density of anhydrite-bearing rocks according to Weijermars *et al.* (1993), g is the acceleration of gravity equal to 9.81 m s^{-2}, Δh is the lateral difference in salt thicknesses that is 2.5 km over the length of the channel that is assumed to be equal to the width of the folded belt, L, which is of ~200 km.

For reasonable viscosities of salts $\eta_{\text{salt}} = 10^{17}$–$10^{18}$ Pa s (Costa & Vendeville 2002) the rate at which the salt escapes towards the front falls between 3 and 50 mm yr^{-1}. These values are consistent with flow rates calculated by McQuarrie (2004). The flow of salt towards

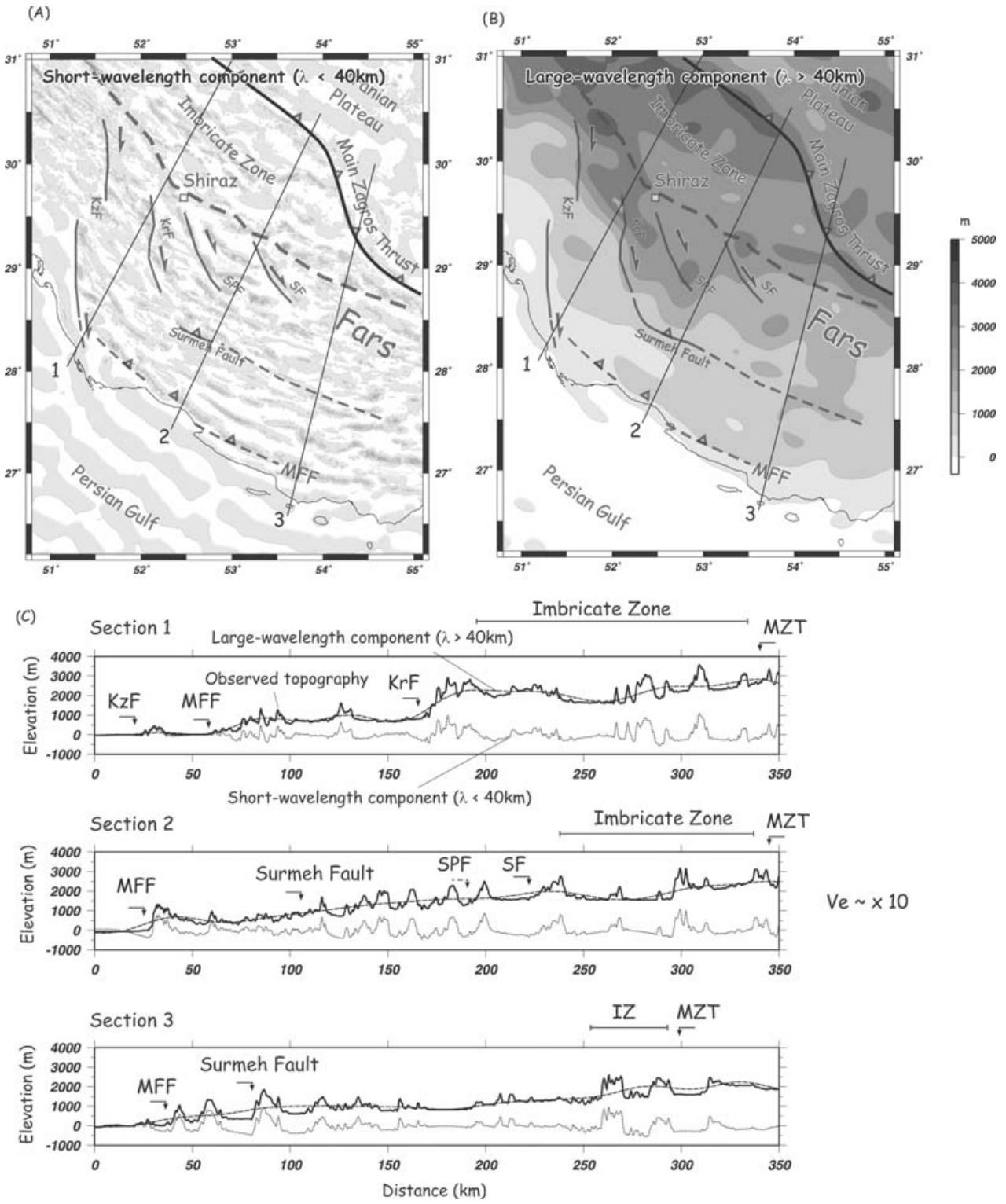

Figure 8. Wavelength analysis of the topography. (a) The short-wavelength components of the topography ($\lambda < 40$ km) shown in map view clearly depicted the succession of local folds in the Fars. (b) The large-wavelength components of the topography ($\lambda > 40$ km) highlight the regional trends, especially that related to the Surmeh/Karebass fault system. (c) Topographic sections along transects 1, 2 and 3 (whose location is also presented in Fig. 3). The profiles show the observed topography (solid lines) and the filtered topography for both large- and short-wavelength components of the topography (dashed and dotted lines, respectively). The main fault zones are well depicted and named. These are the MFF (Mountain Front Fault), SPF (Sabz-Pushan Fault), KzF (Kazerun Fault), KrF (Karebass Fault), SF (Sarvestan fault) and Surmeh (Surmeh Fault). In the northern part of the Fars, the MZT (Main Zagros Thrust) and the Imbricate Zone are also shown.

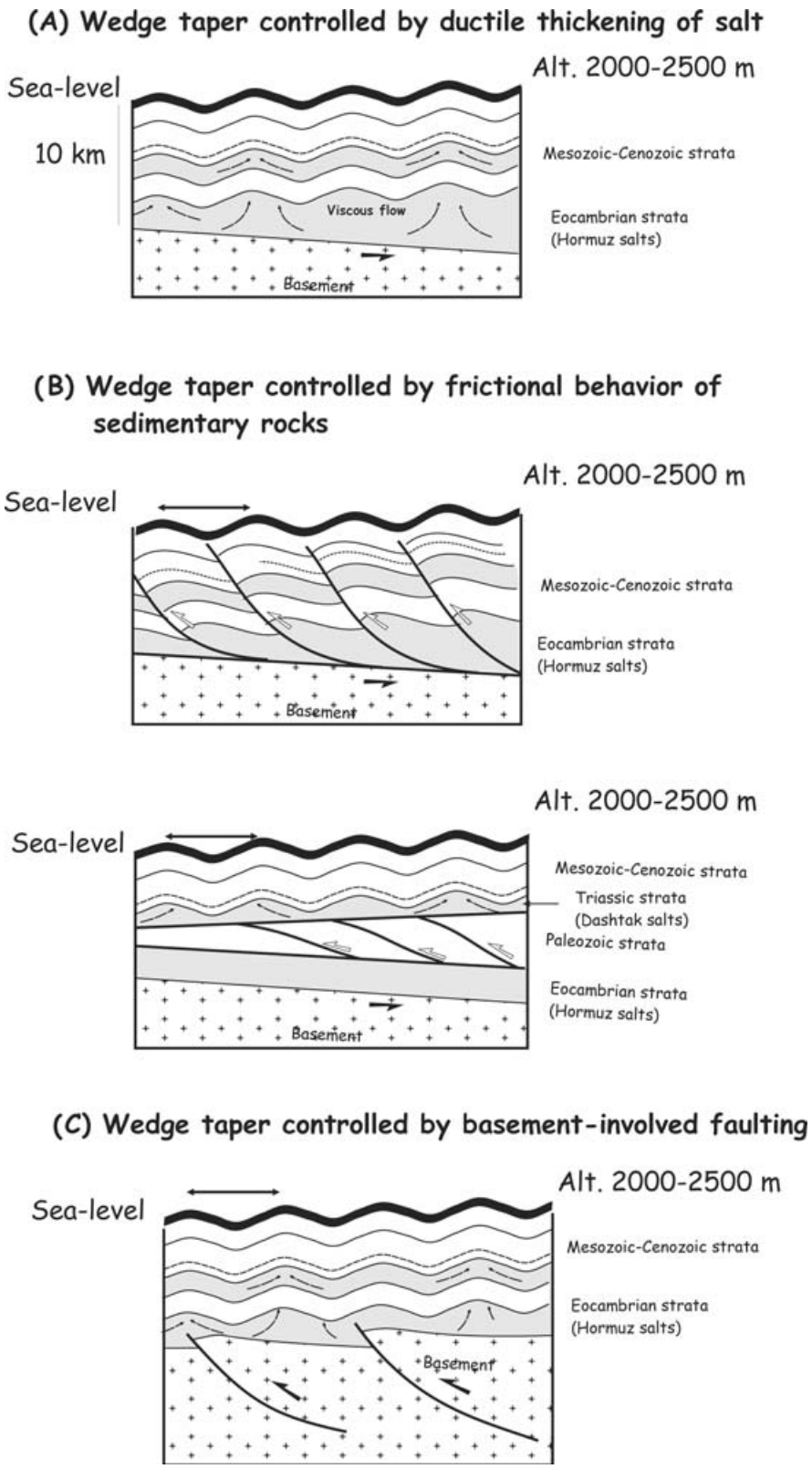

Figure 9. Conceptual structural models involving different crustal levels of deformation and mechanical assumptions that are examined in this study to fit the observed topography. (a) The differential regional topography is assumed to result from the ductile thickening and wedging of the Hormuz Salt. (b) The regional topography is related to brittle deformation in the all sedimentary cover or in the lower part of the competent cover that is detached above the Hormuz Salt in agreement with a thin-skinned style of deformation. (c) This model hypothesizes that the regional topography is created by the brittle deformation of the basement.

the foreland appears to be 10–100 times faster than the average uplift rates. This suggests that the salt cannot maintain the topography but rather will flow towards regions of lower topography, thus rapidly reducing the topography. In other words, such a hypothesis would require that the Hormuz salts thicken 10–100 times faster than the surface topography grows, requiring very rapid rates of shortening compared to the estimates given in introduction. Although such a process may have been efficient in the development of salt accumulation to the southernmost Fars where numerous salt domes are observed, or to explain the Mountain Front Flexure (Bahroudi & Koyi 2003; McQuarrie 2004) the regional topography cannot be satisfactorily reproduced by such a mechanism alone.

4.2 Brittle deformation and imbricate thrusting in the sedimentary cover

We assume in this part that the main mechanism responsible for the growth of the regional topography is the thickening of the cover by brittle deformation above the Hormuz salt (Fig. 9b). This hypothesis of a thin-skinned thrust wedge made of brittle sedimentary rocks detached over the Eo-Cambrian salts will be mechanically tested in Section 5. First, we note that the ratio of the sedimentary layer thickness ($\sim$10 km) to the wavelength of folds (i.e the distance between two successive imbricate thrust slices) is 2–2.5, which is roughly consistent with the ratio of $\sim$3 observed in sand-box experiments for low basal friction wedges (Gutscher *et al.* 1998). A limitation of this model is the lack of fault-ramps at the surface or backthrusts that could explain the symmetry of folds. But these faults may be buried. An alternative explanation is to hypothesize that folding observed at the surface is decoupled from a deeper brittle deformation at an intermediate weak layer in the cover. The local topography can be produced by buckling and eventually symmetrical thrusts and backthrusts ('pop-up' structures typical of low-friction wedges) whereas the deeper part of the sedimentary cover is deformed by sliding along thrust ramps (Fig. 9b). This hypothesis requires a second intermediate décollement that decouples an upper and a lower competent group. If such a layer exists, it should lie between the Cretaceous strata, which are exposed in numerous anticlines of the Zagros, and the Cambrian Hormuz salt. Based on lithologies of Jurassic or Triassic rocks in the Fars, the Dashtak evaporitic Formation is probably a good candidate (Fig. 2).

4.3 Basement thrusting

The last hypothesis considers that shortening in the sedimentary cover is not at the origin of the large-scale topography. Instead, it is the brittle thrusting within the Precambrian crystalline basement that creates the regional topographic slope (Fig. 9c). This hypothesis is supported by both localized and long-lived deformation along several basement fault segments (e.g. Surmeh Fault and MFF) and the distribution of seismogenic activity within the upper brittle crust (Figs 1 and 3). In this interpretation, the cover is completely detached from the basement by sliding plastically along the décollement of the Hormuz formation or by buckling (Fig. 1). The main difference from the previous hypotheses is that the sedimentary cover is not necessarily tectonically thickened.

5 CRITICAL WEDGE MODELLING

The critical wedge theory as it was defined in reference papers (Davis *et al.* 1983; Dahlen 1984; Dahlen *et al.* 1984; Dahlen 1990) assumes that the overall shape of a fold-and-thrust belt can be reproduced by a wedge of rocks having a brittle behaviour. This brittle wedge is translated above a décollement horizon whose friction is necessarily lower than the internal friction of the wedge. For Coulomb critical wedge models, the strength of rocks within the wedge is limited by a Coulomb failure criterion. When the state of stress within the wedge attains a critical value, defined by its internal friction, a critical taper is achieved. The critical wedge taper is defined as the sum of the dip of its base β that is taken positive towards the hinterland and the dip α of its upper topographic slope, which is positive towards the foreland.

Hereafter, we adopt a critical wedge approach to compare the theoretical shape of the Zagros tectonic wedge with the observed topographic slope. Taking into account the previous discussion on the relation between topography and possible structural styles at depth we examine two end-member possibilities. The first model refers to a wedge of brittle sedimentary material having pressure-dependent frictional behaviour that is detached above a viscous décollement represented by the Hormuz Salt. The second model aims at fitting the observed regional topography to a thick-skinned wedge involving the whole upper crust (Meso-Cenozoic sediments and Precambrian basement) that is mechanically decoupled above a thermally weakened lower crust. In this latter model we implicitly neglect the decoupling between the cover and the basement in contributing to the regional-scale topography. This approximation will be justified in the following.

5.1 Shallow brittle–ductile wedge of sedimentary rocks

Critical wedge theory has been successfully applied to many fold-and-thrust belts such as the Taiwan Western Foothills or the Himalayas (Davis *et al.* 1983) and we can consider that most geometric and kinematic characteristics of foreland fold-thrust belts having significant basal friction can be reproduced to a first order by this theory. However, for fold-and-thrust belts whose basal décollement is in a ductile horizon, like the Zagros folded belt, the extreme weakness of salt has important effects on the shape and behaviour of the fold-and-thrust belts. For instance, they have very narrow tapers $<1^\circ$ and are characterized by the absence of preferred vergence of folding or thrusting.

A discrepancy is usually found between the very low taper depicted in such salt-based wedges and the predicted taper using Coulomb critical wedge. This has led Davis & Engelder (1985) to redefine the 'criticality' of brittle wedges on the basis of a plastic pressure-independent behaviour of the décollement instead of a frictional pressure-dependent criterion, that more reliably reproduces the behaviour of salts. Some analogue models dealing with the geometry and propagation of fold-and-thrust belts overlying a weak ductile décollement have successfully reproduced such very low tapers, symmetrical folding as well as local diapirs that characterized such thrust belts (Costa & Vendeville 2002) in agreement with taper defined by Davis & Engelder (1985).

5.1.1 Model parameters: friction of sedimentary rocks and salt viscosity

In this model, stresses within the sedimentary cover, in the upper 10 km of the crust, is limited by brittle fracture represented by a Coulomb criterion (Fig. 10). As the deformation of rocks takes place at shallow crustal depths ($<$10 km) the averaged internal friction coefficient μ gs generally high of 0.85 (i.e. angle of internal friction of 40°) in agreement with Byerlee's law (Brace & Kohlstedt 1980).

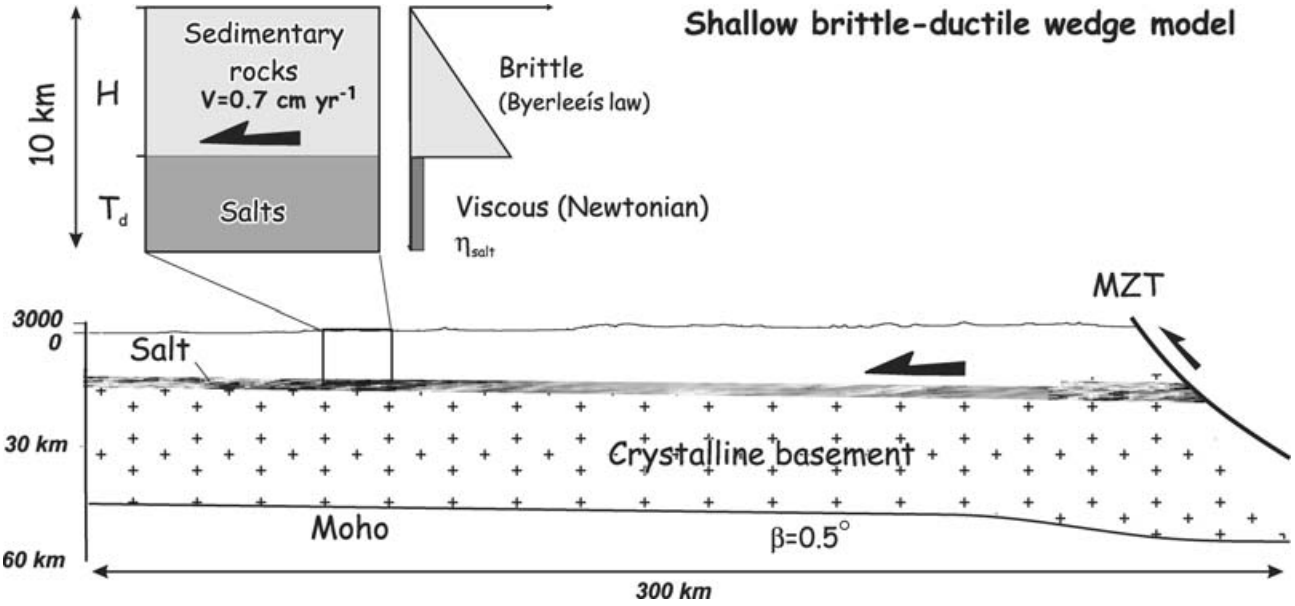

Figure 10. Model of a brittle–ductile thin-skinned critical wedge. A brittle frictional behaviour is assumed for folded sedimentary cover that is translated above a viscous (Newtonian) décollement. This model is consistent with structural style proposed in Fig. 9(b). See text for the description of parameters and material constants.

But in order to test a wider range of friction we extent to angle of internal friction to 30°. The cohesion is set to zero.

In contrast, even for low crustal depths, an evaporitic décollement such as the Hormuz salts formation has almost no strength and will flow (Dahlen 1990). As noticed by Jackson *et al.* (1990) and Weijermars *et al.* (1993) at low stresses and in the presence of a very small amounts of water (0.05 per cent is sufficient) diffusional creep prevails and salt behaves as a Newtonian fluid with a viscosity independent of stress or strain rates but dependent on temperature. This behaviour has been successfully used in modelling gravitational instability of salts as fluid instability to explain the formation of 'salt domes' (Jackson *et al.* 1990) or in analogue modelling of fold-thrust belts overlying extremely weak décollement (Cotton & Koyi 2000; Costa & Vendeville 2002). Based on observed diapiric instabilities of the Eocene salt layer studied in the Great Kavir desert, some values for salt viscosities in the Zagros have been indirectly proposed (Jackson *et al.* 1990). Those values are very low of the order of 10^{15} Pa s for the Hormuz salt mostly because it deformed at depths below 5 km. In contrast, values of salt viscosity used in analogue modelling to reproduce the shape of fold-thrust belts are generally higher as they are limited to available analogue materials such as silicone putty that assumes high effective viscosities up to 10^{18} Pa s (Cotton & Koyi 2000; Costa & Vendeville 2002). Numerical approaches use consistent viscosities of about 10^{17}–10^{18} Pa s (Turcotte & Schubert 1982). Accordingly, we chose viscosities of salts comprised between 10^{17} and 10^{18} Pa s. Those values are probably upper bounds if we consider that the Hormuz salt is deforming at depths below 8–10 km.

5.1.2 Analytical model

We adopt equations and approximations that predict the critical taper for salt-based wedges (Davis & Engelder 1985). These authors extended the model of Davis *et al.* (1983) for thrust wedge that include pressure-independent plastic décollement at the base. The modified critical taper for such fold-thrust belt is

$$\alpha + \beta = \frac{\beta + \left(\frac{\tau_b}{\rho_{\text{sed}} g H}\right)}{1 + (1-\lambda)\left(\frac{2}{1/\sin(\phi)} - 1\right)}, \quad (1)$$

where α is the topographic slope of the wedge, β is the slope of the basement, λ is the pore fluid pressure ratio within the wedge, τ_b is the yield stress of the salt, ϕ is the angle of internal friction (between 30° and 40°), ρ_{sed} is the average volumetric mass of the wedge and H is the thickness of the wedge. Due to the lack of information about pore fluid pressure ratios in the Zagros we tested different values of λ for 0 (dry sediments), 0.4 (hypothesizing that the sediments are wet) and 0.9 (lithostatic pore pressure). The pore fluid pressure for salts is set to zero.

In the case of ideal frictional behaviour (Coulomb criterion) the shear stress resisting the sliding of the sedimentary cover is pressure dependent but is independent of the strain rate. For low viscosity of the basal décollement the strength is independent of the thickness of the brittle cover but depends on the thickness of the viscous layer and shear-strain rate (Weijermars *et al.* 1993). The forces in the salt resisting the advancement of the wedge are believed to be accommodated by simple shear (Fig. 10) of the whole viscous layer similar to a Couette flow (Turcotte & Schubert 1982). The basal shear stress τ_b in the basal décollement is thus given by:

$$\tau_b = \eta_{\text{salt}} \frac{V}{T_d}, \quad (2)$$

where η_{salt} is the (Newtonian) viscosity of the Hormuz salts, T_d is the thickness of the viscous layer and V is the displacement rate imposed at the rear of the folded belt. The present-day displacement field based on GPS studies gives a shortening rate of 0.7 cm yr^{-1} (Vernant *et al.* 2004). For geological rates, amounts of shortening derived from restored sections yield a long-term shortening comprised between 70 km (McQuarrie 2004) and 34 km (Sherkati & Letouzey 2004). Assuming that the phase of maximum shortening occurred between 5 and 10 Ma (i.e. Upper Agha Jari) we estimate

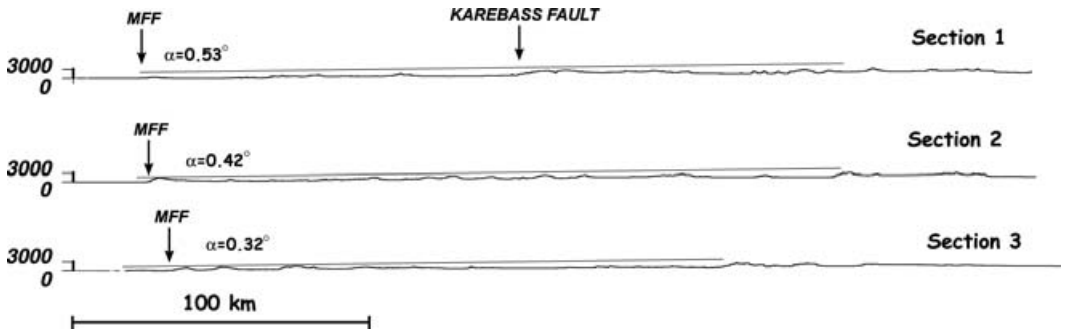

Figure 11. Topography derived from SRTM data and estimated topographic slopes along sections presented in Fig. 3.

slightly lower rates of shortening for the Fars area in the range from 0.3 to 1.4 cm yr^{-1}. An average value of 0.7 cm yr^{-1} for the shortening rates is reasonable and was set for all models. The shear stresses in the salt layer is tested for different values of the thickness of the Hormuz formation (0.5, 1 and 2 km) usually considered in the Zagros (Jackson *et al.* 1990).

To constrain the value of the décollement dip β (basement top) we assume that its geometry mimics that of the Moho. The deepening of the Moho beneath the Fars is inferred from seismological constraints on the crustal structure and inversion of gravity data. Those data show that the Arabian plate dips at 1° (Snyder & Barazangi 1986) and perhaps less ∼0.6° (Hatzfeld *et al.* 2003). This gently deflected Moho is consistent with the fact that the Arabian continental margin is relatively strong as suggested by its elastic thickness of 50 km (Snyder & Barazangi 1986). The slope of the basement β derived from restored sections (McQuarrie 2004) gives a consistent estimates of 0.5°. Consequently, a value of 0.5° has been set for the basement dip β. Finally, using eq. (1) we compute the mean surface slope angle α that we compare to the observed topographic slopes (Figs 11–13).

5.1.3 Model results

The average surface slopes across the Zagros folded belt have been estimated within the actively deforming portion of the Fars (Fig. 11). As the Imbricate Zone is remarkably aseismic and topographically flat (Figs 3 and 11) this part was not considered. Along the strike of the belt, the best-fitting topographic slopes obtained decrease from 0.5° to 0.3° towards the south (Fig. 11). The shear stresses at the base of the wedge, derived from eq. (2), vary between 11 and 443 kPa. These values are consistent with typical values of the yield strength of salts estimated in other fold-thrust belts, for example, the Salt Range–Potwar Plateau, or based on laboratory experiments (e.g. Jaumé. & Lillie 1988). The lowest shear stress is obtained for a salt décollement having a low viscosity of 10^{17} Pa s and a thickness of 2 km. The highest value is for a higher viscosity of 10^{18} Pa s and thin salt layer of 0.5 km.

In Fig. 12 we show the topographic slopes computed using eq. (1) and plotted against a range of angles of internal friction. The role of the basal shear stress and pore fluid ratio is also taken into account. The 'steepest' topography (∼0.002°) is observed of course for the highest basal shear stress ∼443 kPa and the lowest angle of internal friction of 30° considered in these tests. The lowest topographic slope (−0.11°) is obtained for a basal shear stress of 11 kPa and an angle of 40°. It is clear, despite relatively important variations between each model, that the topography predicted is essentially flat (Figs 12 and 13). Modelling reveals that the wedge shape is

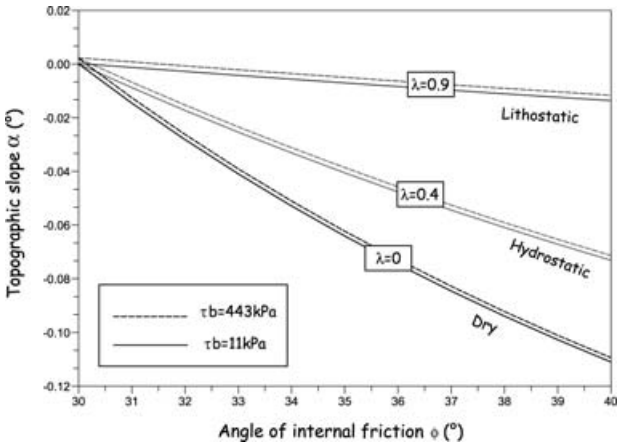

Figure 12. Topographic slopes for brittle wedges overlying a plastic décollement (salt-based wedges) calculated for different values of the internal friction of rocks. The slopes are given for maximum/minimum values of the basal shear stresses (τ_b) in the salt décollement. Even for lithostatic conditions in the wedge ($\lambda = 0.9$) the topographic slopes remain slightly negatives (hinterlandward dips). Only for some internal friction angles (<31°) very low positive topographic slopes are predicted. Note that increasing the pore fluid ratio extends the domain of positive topographic slopes for greater internal friction. Based on this graph it is clear that such types of wedges are essentially topographically flat and are consequently not able to fit the observed topographic slopes of 0.3°–0.5° (see Fig. 11).

weakly sensitive to salt viscosities. In contrast, it is more dependent on internal frictions of rocks and pore fluid pressure ratios. The best solutions we obtain by varying all these parameters are still unable to reproduce the observed topographic slopes of 0.3°–0.5°. In fact, in order to reproduce the required topographic slopes of 0.3°–0.5° there are two extreme cases:

(1) the basal shear stress in the salt should be at least 100 MPa and/or

(2) the internal friction angles should be less than 18°.

The first hypothesis is unrealistic as it would require viscosities of the order of 10^{20} Pa s for salt at depths of 8–10 km. The second hypothesis requires rocks with extremely low friction angles that are not consistent with the brittle strength of most rocks in compressional regime.

In the example of the Zagros, the sedimentary cover and the underlying salts are both remarkably thick. As a result the ratio $\tau_b/\rho_{sed}\, gH$ is very small of the order of 10^{-3}. This reveals that

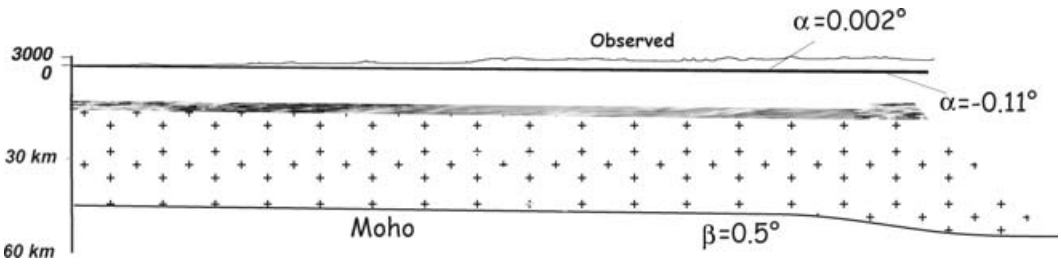

Figure 13. Plot in cross-section of the maximum (positive) and minimum (negative) topographic slopes obtained for different pore fluid pressure, viscosities and thickness of salts (see Fig. 12). The topographic slopes predicted are approximately zero. Comparison with the observed topography indicates that the hypothesis of salt-based critical wedges (Davis & Engelder 1985) is not able to reproduce the observed topography. The salt is too weak to build the observed topography.

when a thick (relatively to its overburden) layer of salt forms the basal décollement it is generally too weak and cannot support the growth of significant topography.

Other natural examples of salt-based fold-thrust belts whose topographic slope is currently zero (or was approximately zero based on restored cross-sections) are the Salt Range–Potwar Plateau (Jaumé & Lillie 1988), the south central Pyrenean belt (Meigs & Burbank 1997) and the North Apennines (Ford 2004). However, at least one natural example exists for which this statement is not valid: the Mediterranean Ridge, a marine accretionary wedge that developed in close relation with a décollement in evaporitic sediments (Messinian salt). It currently shows a surface angle that is low 0.2°–0.3° but not zero for a décollement that dips 1° on average (e.g. Kukowski *et al.* 2002). This case may be tentatively explained by the less important cover thickness above the salt with respect to the Zagros. So the ratio $\tau_b/\rho_{sed}\,gH$ in eq. (1) may become not negligible thus allowing the support of a significant topography.

Ford (2004) recently examined the relation between the topographic slopes and the angle of the décollement in a number of salt-based wedges. She concluded in suggesting that the topography is representative of the strength of the basal décollement but the dip of the basement is likely to be related to flexure of the lower plate. Indeed, β can be controlled by different factors such as subcrustal loads, additional in-plane forces or variations of the flexural rigidity (Burov & Diament 1995). The eq. (1) (see also Fig. 12) suggests that in order to maintain their topography as β increases (other parameters kept constants), salt-based wedges should increase, for instance, their averaged pore fluid pressure ratio.

5.2 Thick brittle–ductile crustal wedge

The last solution is to consider a critically tapered wedge involving the basement consistent with structural model of Fig. 9(c). In this model, the Zagros folded belt mainly results from the thickening of the crystalline basement that is accreted at the front of the MZT above a viscous lower crust (Fig. 14). There is no theoretical limitation in applying the critical wedge taper model to the whole crust. However, some modifications are required to extend the theory to critical wedges extending down to the ductile lower crust whose viscosity is dependent on temperature and pressure. As proposed by

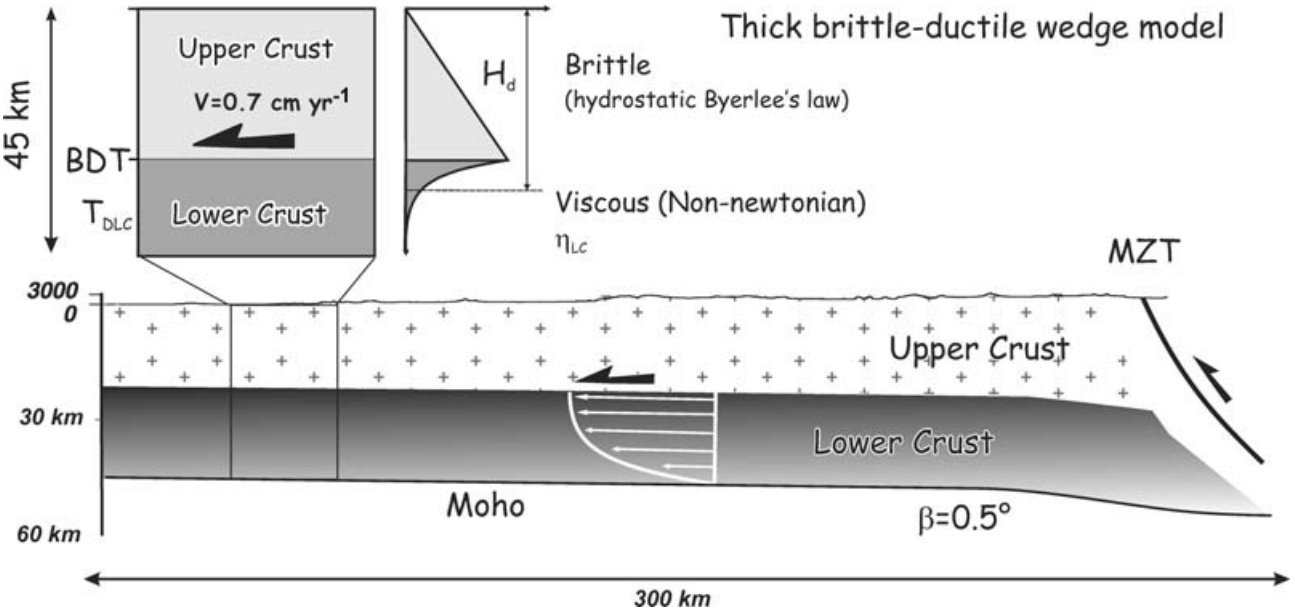

Figure 14. Model of thick brittle–ductile critical wedge. A frictional behaviour is assumed for the upper crustal rocks (see text for parameters). The upper crust is accreted at the front of the MZT above a lower crust with a non-Newtonian viscous behaviour. BDT: brittle–ductile transition; T_{DLC}: thickness of the ductile lower crust, H_d: the depth at which the upper brittle crust is effectively detached from the mantle. This model reproduces the structural style proposed in Fig. 10(c).

Chapple (1978) or Williams *et al.* (1994) we model the wedge taper as being approximately equal to the ratio of the applied basal shear stress to the strength of the material at the base of the wedge.

5.2.1 Yield stress profiles in the Arabian continental margin

A homogeneous brittle property of rocks is assumed in the wedge, so that the role of the viscous Hormuz salts at the base of the cover is neglected. The conditions for brittle failure in the lithosphere are mostly independent of rock type and temperature but are strongly controlled by pressure (Byerlee 1978). The brittle strength for a compressional regime is given by:

$$\sigma^d_{\text{brittle}}(z) = 2\left[C + \rho_{\text{crust}} g z (1-\lambda)\left(\frac{\sin\phi}{1-\sin\phi}\right)\right], \quad (3)$$

where σ_{brittle} is the brittle deviatoric yielding stress, z the depth, ρ_{crust} the average density of the overburden, which is 2700 kg m^{-3}, g the acceleration of gravity, $C = S(\frac{\cos\phi}{1-\sin\phi})$ is the uniaxial compressive strength (Jaeger & Cook 1979), S is the cohesion, ϕ is the angle of internal friction and λ the pore fluid ratio. Even though this formulation constitutes a lower bound for the failure of most rocks, *in situ* stress measurements in deep boreholes have indicated that the strength of continental crust is essentially limited by the friction on favourably oriented pre-existing fractures with nearly hydrostatic pore-pressure gradient (Zoback & Healy 1992; Brudy *et al.* 1996). Consequently, we adopt more reliable hydrostatic conditions ($\lambda = 0.4$) for the brittle profile. Below a depth of 10 km, we chose an averaged internal friction coefficient μ of 0.6 (i.e. angle of internal friction $\phi = 30^\circ$) and the cohesion is 60 MPa in agreement with Byerlee's law.

The main question concerns the mechanical behaviour to adopt for the lower crust. According to the deepest earthquakes observed by Tatar *et al.* (2004) at 18 km and the depth distribution of earthquakes shown by Maggi *et al.* (2000) the aseismic part of the crust is probably deeper than 20 km. At such depths, crustal brittle deformation is probably no longer active and dislocation creep predominates in the lower crust. The behaviour of the lower crust is thus better approximate by a non-Newtonian fluid with a viscosity varying with depths and dependent on strain rate and temperature. Laboratories experiments indicate that flow for most rocks and minerals of the lithosphere results from a thermally activated dislocation creep process (Brace & Kohlstedt 1980). The deviatoric yielding stresses for dislocation creep follow a power law given by:

$$\sigma^d_{\text{ductile}}(z) = \left(\frac{\dot{\varepsilon}}{A}\right)^{1/n} \exp\left(\frac{H}{nRT(z)}\right), \quad (4)$$

where n, A and H are experimentally determined material constants (Table 1). In order to cover a wide range of viscosities in the lower crust we test different rock types such as quartzite for weak lower crust and more mafic composition like diabase, quartz-diorite or granulite for stronger lower crust. The choice of mafic rheologies for the lower crust of the continental lithosphere of Arabia requires some explanation. The growth of the continental lithosphere is often modified by thermal and metamorphic events that alter the lithology of the lower crust. For instance, Déverchère *et al.* (2001) suggested a change in the composition of the lower crust into diabase (gabbroic composition) or granulite beneath the Baikal rift system as a consequence of the emplacement of calc-alkaline bodies during the Palaeozoic. Intraplate volcanics events and underplating have been also described at young continental margin like the Chinese continental margin justifying the choice of a mafic lower crust to maintain a substantial strength of the Eurasian plate at Taiwan (Mouthereau & Petit 2003). In the case of the Arabian lithosphere such lithologies are suggested by the presence of Proterozoic calc-alkaline lavas described in the Central Arabian shield (Roobol *et al.* 1983) justifying the test of our model with diabase (gabbroic composition) or granulite lithologies.

Table 1. Parameters of dislocation creep for lithospheric rocks and minerals adopted for computation of yield stress envelopes (Goetze 1978; Hansen & Carter 1982; Wilks & Carter 1990).

Rheology	A (Pa^{-n} s^{-1})	H (kJ mol^{-1})	n
Quartzite	5×10^{-12}	190	3
Quartz-diorite	1.2×10^{-16}	212	2.4
Diabase	6.31×10^{-20}	276	3.05
Mafic granulite	8.8×10^{-22}	445	4.2

A ductile yield profile is calculated for each type of rocks using eq. (4). At a given depth, the way the crust deforms (brittle or ductile) is controlled by the lower differential stress for yielding (Fig. 15). The lack of heat flow data does not allow an accurate estimation of the crustal geotherm. So we adopt an average cold gradient of 10–15°C km^{-1}, which neglect the contribution of radiogenic heating in the upper crust but which is consistent with a temperature at the Moho of 450–675°C. Such a low gradient is consistent with a 500-Ma-old continental margin (Burov & Diament 1995) and is also consistent with Moho temperature required to allow continental subduction (Toussaint *et al.* 2004). The Moho depth in the Zagros folded belt has been obtained from receiver function analysis (Hatzfeld *et al.*

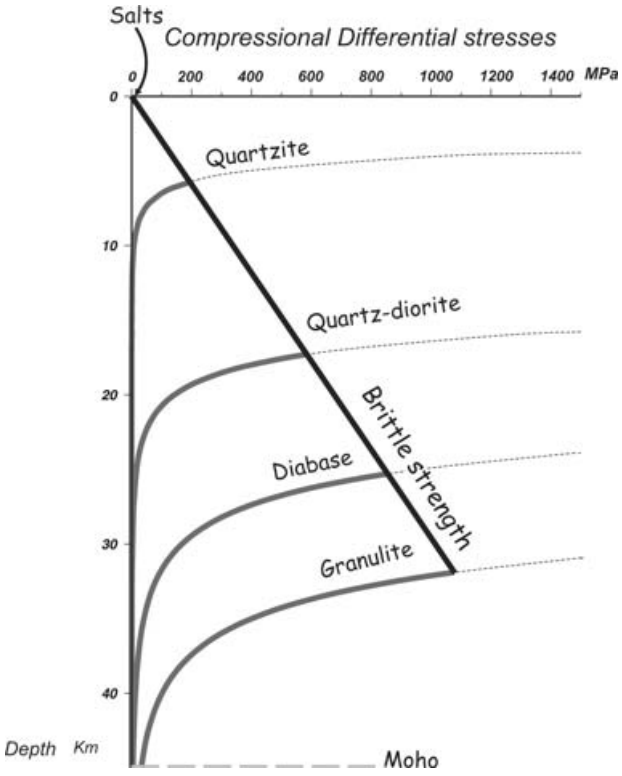

Figure 15. Yield stress envelopes in the Arabian crust calculated for a geotherm of 15°C km^{-1} and different rocks whose rheological parameters are presented in Table 1. The brittle strength is calculated for hydrostatic state (pore fluid ratio of 0.4). For comparison we also mentioned the strength of the salt.

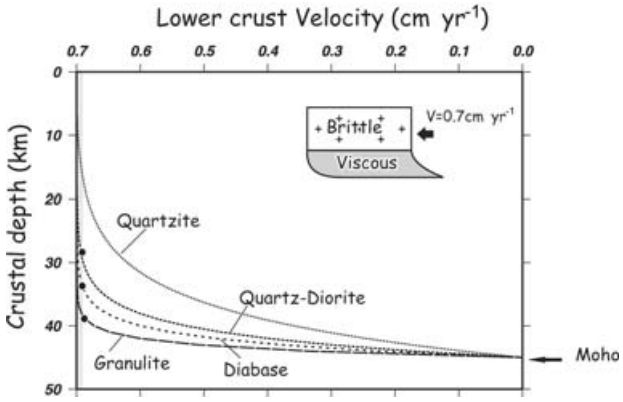

Figure 16. Velocity profiles in the lower crust for different rock type. The velocity in the lower crust is controlled by the non-Newtonian behaviour of rocks. The depth at which the upper brittle crust is effectively detached from the mantle is H_d. Above this depth, the crust is ductile, but its velocity is similar to that in the brittle upper crust. For depths greater than H_d the upper crust is considered as detached from the mantle.

2003). It shows a crustal thickness of 45 km and a thickness of the lower crust, which is approximately 25 km.

Yield stress envelopes first show that the use of quartzite would imply that the upper crust flows at depth of 7 km, which disagrees with deeper earthquakes down to 18 km (Tatar *et al.* 2004). By contrast, for other rheologies a good consistency is found between depth distribution of earthquakes and the brittle strength of the crust. The depths of the brittle–ductile transition (BDT) are 18, 25 and 31 km for quartz-diorite, diabase or granulite, respectively. Hence, we consider that these rocks can satisfactorily reproduce the deformation pattern of interest.

5.2.2 *Velocity and shear stress at the wedge base*

In order to estimate the shear stress at the wedge base, we assume that the resisting forces in the lower crust are represented by simple shear of the lower crust consistent with a Couette flow (Turcotte & Schubert 1982). Because the viscosity obeys a power law, the velocity profile within the ductile lower crust does not vary linearly with depth. This implies that the upper portion of the viscous lower crust of higher strength is kinematically coupled to the upper brittle crust. A solution for Couette flow governed by a power law has been proposed by Turcotte & Schubert (1982). We compute the velocity profile for Couette flow in the different rock type (Fig. 16). The boundary conditions involve a strain rate of zero at the bottom of the viscous channel, that is, at the Moho depth whereas the velocity at the upper boundary, that is, in the upper brittle crust is fixed to 0.7 cm yr^{-1}, which is equal to the strain rate in the upper crust ε_0 of 9×10^{-15} s^{-1}. To determine the depth location of the intracrustal decoupling between the upper competent brittle–viscous layer and the lower viscous crust we define the depth H_d. It corresponds to the depth above which the crustal velocity is about 99 per cent that imposed at the rear. This depth H_d is different for each type of rocks. Above H_d the displacement of rocks is mainly dependent on the strength of rocks (brittle or viscous) close to the BDT. Below H_d, the viscous flow is mainly dependent on low viscous strengths. The thickness of the wedge corresponds to H_d, which is the depth at which the upper crust is effectively detached from the mantle.

The effective viscosity at depth H_d can be derived from the following relation

$$\eta_{\text{eff}}(z) = \frac{\sigma^d_{\text{ductile}}(z)}{2\,\dot{\varepsilon}(z)}, \tag{5}$$

in which the strain rates $\dot{\varepsilon}(z)$ within the ductile channel have been calculated using velocities for non-Newtonian rheologies shown in Fig. 15. Then because the shear stresses at the wedge base H_d (Table 2) is

$$\tau_b = \eta_{\text{eff}}\,\dot{\varepsilon}(z), \tag{6}$$

the basal shear stresses at the depth H_d can be simply obtained using

$$\tau_b = \frac{\sigma^d_{\text{ductile}}}{2}. \tag{7}$$

Assuming that the critical taper of a brittle–ductile wedge is the ratio of the basal shear to the brittle strength of the material at the wedge base, the critical wedge taper $\alpha + \beta$ for a brittle wedge overlying a ductile base can be approached by:

$$\alpha + \beta = \frac{\rho_{\text{crust}} g H_d \beta + \tau_b}{\rho_{\text{crust}} g H_d + \sigma^d_{\text{brittle}}}, \tag{8}$$

adapted from (Williams *et al.* 1994).

5.2.3 *Model results*

Based on depths H_d derived from the velocity profiles presented in Fig. 16, we obtain effective viscosities of 3×10^{20}, 5×10^{21}, 10^{22} Pa s for quartz-diorite, diabase or mafic granulite, respectively (Table 2). We then derive basal shear stresses of about 1.8, 24.5 and 48 MPa on the intracrustal décollement.

Taking into account the values of the maximum brittle strengths attained at the BDT and the geological constraints on the gentle dip of the Moho, we compute three different wedge tapers for each composition of the lower crust (Fig. 16 and Table 2). Assuming a quartz-diorite rheology, we obtain a negative value of α of -0.42° (taper angle of 0.08°), the lower crust is too weak and cannot maintain the observed topography (Fig. 17). In contrast, when using stronger rheologies like diabase and granulite we are able to produce positive topographic slopes of 0.4° and 0.86°, respectively (equivalent

Table 2. Results of thick-skinned brittle–ductile wedge modelling. BDT is the depth of the brittle–ductile transition. H_d is the depth of effective crust-mantle decoupling, η_{eff} is the effective viscosity of the lower crust at depth H_d, τ_b is the corresponding basal shear stress in the viscous lower crust, τ_b/Δ is the ratio of the basal shear stress to the brittle strength in the upper crust, $\alpha + \beta$ is the wedge taper and α the topographic slope.

Rheology	BDT (km)	H_d (km)	η_{eff}(Pa s)	τ_b(MPa)	τ_b/Δ	$\alpha + \beta$	α
Quartz-diorite	18	29	3×10^{20}	1.8	0.003	0.08°	-0.42°
Diabase	25	33	5×10^{21}	24.5	0.04	0.9°	0.4°
Mafic granulite	31	39	10^{22}	48	0.05	1.36°	0.86°

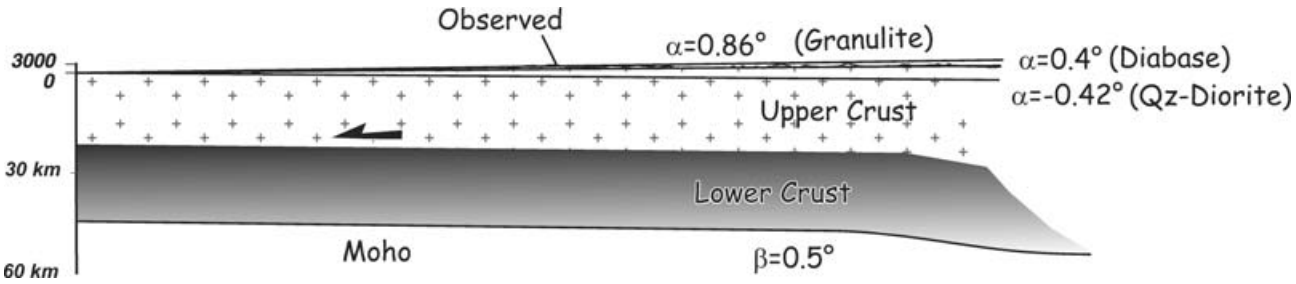

Figure 17. Model results. Topographic slopes obtained for different compositions of the lower crust (granulite, diabase or quartz-diorite). The values of the effective viscosities and shear stresses for granulite and diabase are sufficient to reproduce the observed topographic slopes in the Fars.

to tapers of 0.9° and 1.36°) consistent with the observed topography (Fig. 17). Although not shown for clarity, it is possible to obtain a better fit by modifying, for instance, the pore fluid pressure or the internal friction in the brittle portion of the crust.

As a result, we suggest that a thick brittle–ductile wedge that involves the crystalline basement is able, to a first approximation, to reproduce the observed topography. We are aware that these results are based on a very simple analytical modelling that is not able to account for more complex interactions that likely arise from a more realistic elastic–brittle–viscous rheology more sensitive to variations of strain rates or viscosities. We note that rock composition in the lower crust is important and should necessarily comprise sufficiently viscous materials whose rheology is analogous to that of diabase or granulite (5×10^{21}, 10^{22} Pa s, respectively), otherwise the topography would not be supported.

6 DISCUSSION AND CONCLUSIONS

6.1 Basement-involved shortening, topography of the Fars and distribution of deformation

The basement involvement in deformation of the Zagros and especially in the Fars is a controversial point. This possibility was suggested by several authors based on structural/sedimentation relationships (e.g. Egdell 1996) or based on seismotectonics studies (Jackson 1980; Berberian 1995; Talebian & Jackson 2004; Tatar *et al.* 2004). On the other hand, the effect of the spatial distribution of the Hormuz salt has been alternatively proposed to explain partitioning and changes in deformation styles along the strike of the belt (Bahroudi & Koyi 2003). For instance, the MFF has been explained by the reactivation of an inherited basement normal fault (e.g. Falcon 1974; Comby *et al.* 1977; Berberian 1995) or by the abrupt decrease of the salt thickness (e.g. Bahroudi & Koyi 2003; McQuarrie 2004). There is no doubt that both salt tectonics and basement tectonics explained part of its present configuration and deformation styles. But at a larger scale how is the deformation in the cover and the basement partitioned and what mechanisms explain the observed topography?

In this study, we have chosen to examine the observed topography as a starting point to test both hypotheses. In the Fars, the topographic slopes are low (0.5°–0.3°) and decrease regularly towards the southeast. First, we show based on critical wedge theory applied to non frictional salt-based critical wedges (Davis & Engelder 1985) that the assumption of a thin-skinned fold belt detached above a viscous layer of salt is unable to produce the observed topographic slopes. We note that low internal strength of rocks and/or very high yield of salt would be required in the wedge to produce the observed topography. The first hypothesis disagrees with the friction of most rocks in compressional settings and the second possibility is inconsistent with the rheology of salt at such depths (8–10 km).

In a second part we have tested a model of critically tapered brittle–viscous wedge involving the crystalline basement. This model reproduces the observed topographic slopes across the Fars province, better than a shallower sedimentary brittle–ductile wedge alone does. In this model, the lower crust was deformed by simple shear and behaved as an intracrustal decoupling level allowing the accretion of the crystalline basement at the front of the MZT. An average cold crustal geotherm of 10–15°C km^{-1} consistent with Moho temperature of 450–675°C is able to thermally weakened sufficiently the lower crust that flows at depth deeper than 20 km in agreement with the depth distribution of seismicity derived from recent studies (Maggi *et al.* 2000). This study suggests that the shortening and thickening of the Precambrian basement may be a major mechanism controlling the growth of the topography in the Fars. This model further supports predictions from the most recent cross-sections balancing (Molinaro *et al.* 2004; Sherkati 2004), gravity modelling (Snyder & Barazangi 1986) or other studies based on seismotectonic studies (Berberian 1995). So the deformation in the cover seems to have little effect on the growth of the topography even though it may strongly control the deformation styles observed at the surface.

GPS studies have shown that the Zagros accounts for 30–50 per cent of the total convergence between Eurasia and Arabia (Talebian & Jackson 2004). In contrast, only 10 per cent of the convergence is accounted for by the deformation released during earthquakes in the Zagros (Jackson & McKenzie 1988; Jackson *et al.* 1995). This suggests that a significant part of the present deformation in the Zagros is accommodated by aseismic processes in the Arabian crust. If we hypothesize that the current amount of deformation associated with earthquakes was valid in the past it is possible to relate to first order the observed active brittle deformation in the basement with the basement shortening that is required to produce the Zagros topography. If this is confirmed it would imply that the topography of the Zagros is the result of 10 per cent of shortening. This is far from the estimates based on GPS studies or balanced cross-sections. There may be several explanations to this apparent contradiction.

First, as Jackson *et al.* (1995) mentioned the magnitudes of earthquakes ($M_s > 6$) used to compute the seismic deformation account for only 60 per cent of the total deformation released by earthquakes, so 10 per cent is probably a lower bound. Second, our thick-skinned model has been designed for crustal rocks having a frictional behaviour but a more realistic brittle–viscous model should be envisaged. Thirdly, the possibility that the ductile lower crust was thickened aseismically should be considered. In our model this mechanism was not required to produce the topography. But we

note that the ductile thickening of the lower crust has been proposed early by Snyder & Barazangi (1986) based on flexure modelling. We consider the thick-skinned model, able to produce alone the regional topography, as an additional hint for basement thrusting in the Zagros.

6.2 Structural styles in the cover of the Fars: buckling versus faulting

In contrast with the thick crustal wedge model, a model of imbricate thrust sheets in the cover (Figs 9b, 11—13), that are translated above the Eo-Cambrian salts of the Hormuz Formation, reveals that salt strata have viscosities that are too low to support the regional load arising from the overlying cover and consequently to form the topography of the Zagros folded belt. Note that if this is correct, a thick salt layer will not survive as it is squeezed out in less than 1 Ma. We may expect that below some synclines the base of the sedimentary cover directly overlies the basement. The local topography related to monoharmonic folding in the cover appears essentially superimposed on the regional topographic slope that is created by the thickening of the basement. Two different mechanisms can be proposed to explain the wavelength of surface folding.

The first one considers that folding results from the accommodation of deformation along regularly spaced thrust faults rooted to depth in the weak salt décollement. This hypothesis follows the classical description of the Fars folded belt as a thrust wedge sliding above an extremely weak décollement. For such folded belts the compressional stress is much less inclined than in the case of fold belts involving stronger décollements (e.g. Taiwan). The absence of mechanically preferred vergence of thrusts results in symmetrical anticlines and a very narrow taper $<1^\circ$ (e.g. Davis & Engelder 1985). If the compressional stress σ_1 is nearly parallel to the décollement the width of a fold can be easily calculated. The wavelength of the fold at the surface is given by the distance between the thrust and the backthrust that produce folding $\sim$20–25 km in our case. We found that very low internal friction angles of 12°–24° ($\mu = 0.2$–0.4) are required to produce such wavelengths, which disagree with the friction of most rocks in compressional settings. These estimates would not be conclusive of course if rotation of thrust faults has occurred. But in that case, all thrust faults would have been rotated by the same amount across the whole Fars. This is not consistent with analogue modelling of thrust above a ductile substrate showing that the wavelengths of folding regularly decreases as the thrust dips increase towards the backstop (e.g. Bahroudi & Koyi 2003).

The second hypothesis assumes that the sedimentary cover behaves as a brittle–elastic medium that may buckle above a layer with very low viscosity and density like that of salt. This solution has the advantage of neither requiring the macroscopic failure of the sedimentary rocks nor producing any regional topographic slope. Under sufficient differential stresses, the sedimentary rocks will bend periodically above viscous salt. The wavelength λ for buckling an elastic layer of thickness H as a function of the fiber stresses σ (or horizontal forces) is $\lambda = \sqrt{\frac{\pi^2 E H^2}{\sigma(1-\upsilon^2)}}$ (Turcotte & Schubert 1982), where the elastic properties of the competent medium are described by a Young's modulus E of 10^9 Pa and a Poisson coefficient ν of 0.25. Because the sedimentary layer is brittle–elastic, the effective elastic thickness of the sedimentary layer can dramatically reduce to roughly H/2 (e.g. Burov & Diament 1995). Given a sedimentary cover thickness H above the décollement of about 8 km, we obtain buckling wavelengths of 23–29 km, which are in the range of observations for acceptable stresses of the order of 200–300 MPa and for friction coefficients that are consistent with Byerlee's law. This suggests that a model of buckling of the sedimentary cover fits the wavelength of folding better than a fault-related folding model does. We conclude that bulking is a reliable mechanism to explain the observed folding.

6.3 Implications for the migration of deformation

Few data are available across the Zagros fold belt concerning the timing and kinematics of its long-term propagation. Some regional studies based on the recognition of local syn-folding unconformities (Hessami *et al.* 2001) have proposed that folding started at the end of the Eocene and migrated progressively in-sequence southwards. However, sand-box experiments have shown that the sequence of deformation in salt-based wedges usually does not follow a simple in-sequence scheme (Costa & Vendeville 2002; Bahroudi & Koyi 2003; Smit *et al.* 2003). Isopachs and field observations presented in this study have allowed us to reach this general conclusion. For instance, the local lack of the Mishan and Gashsaran Formations suggests uplift in the vicinity of the MFF that may be tentatively related to the direct or indirect activity in this buried basement reverse fault. Additionally, isopachs reveal that the Mishan depocentre is located in the footwall of the Surmeh Fault. This may suggest that the Surmeh Fault might have been active at that time and produced flexure of the southernmost Fars by thrust loading. Because the MFF and the Surmeh fault are both major active basement reverse faults, tectonic inversion of the rifted continental margin in the Zagros foredeep might have occurred as soon as the Langhian-Serravalian at 16–11 Ma. Such an early stage of compression controlled by the reactivation of pre-existing faults in the foreland has already been described in other forelands, such as in Taiwan (e.g. Lacombe & Mouthereau 2002; Mouthereau & Petit 2003). This early episode of basement-involved deformation probably did not result in the development of regional-scale relief across the Zagros fold belt. It is the consequence of the attenuation of orogenic stresses into the foreland along favourably oriented inherited features. So this early stage of basement involvement in the Zagros foredeep does not directly correspond to the propagation of the thick-skinned thrust wedge which should be active northwards (e.g. in the Imbricate Zone) at that time.

The folded synorogenic deposits of the Agha Jari Formation reveal that the construction of the Fars was achieved after a second more important episode of shortening 10 Ma ago (see Introduction). If buckling was the main mode of deformation in the cover we expect that folds grew simultaneously as soon as the required critical stresses was attained throughout the folded belt. This is supported by the numerous intraformational unconformities observed in the Agha Jari formation (e.g. Homke *et al.* 2004). No important differential regional topography is required at that time. Hence no important changes in the conditions of deposition are required across the belt. The unconformity between the Pleistocene fluvial deposits of the Bakhtyari Formation and the folded Meso-Cenozoic layers finally indicates that deep-seated thick-skinned deformation occurred after the main episode of deformation in the cover thus giving birth to the present-day topography in agreement with a model recently proposed by Molinaro *et al.* (2005). It is important to note that the faulting in the basement has resulted in the folding of the upper décollement in the Hormuz salt. However, the decoupling in the salt is so efficient that basement faults did not cut the salt décollement completely except for some very active basement faults like the Surmeh Fault, otherwise the shortening would not be possible in the cover.

Finally, the involvement of the basement provides mechanical and kinematic constraints that should be accounted for cross-sections balancing and further assessing the evolution of Zagros at crustal or lithospheric scales.

ACKNOWLEDGMENTS

This work has been supported by the Middle East Basin Evolution (MEBE) program. The authors thank the Geological Survey of Iran for its support for fieldwork and especially A. Saidi, P. Navabpour and S. Kargar. The authors would like to thank E. Burov for constructive discussions about model parameters. We are greatly indebted to M.A. Gutscher and M. Ford for their thoughtful reviews that led to significant improvement of the final version of the manuscript.

REFERENCES

Bahroudi, A. & Koyi, H.A., 2003. Effect of spatial distribution of Hormuz salt on deformation style in the Zagros fold and thrust belt: an analogue modelling approach, *J. Geol. Soc. London,* **160,** 1–15.

Berberian, M., 1995. Master 'blind' thrust faults hidden under the Zagros folds: active basement tectonics and surface tectonics surface morphotectonics, *Tectonophysics,* **241,** 193–224.

Berberian, M. & King, G.C.P., 1981. Towards a paleogeography and tectonic evolution of Iran, *Can. J. Earth Sci,* **18**(2), 210–265.

Blanc, E.J.-P., Allen, M.B., Inger, S. & Hassani, H., 2003. Structural styles in the Zagros simple folded zone, Iran, *J. Geol. Soc. London,* **160,** 401–412.

Brace, W.F. & Kohlstedt, D.L., 1980. Limits on the lithospheric stress imposed by laboratory experiments, *J. geophys. Res.,* **85,** 6248–6252.

Brudy, M., Zoback, M.D., Fuchs, K., Rummel, F. & Baumgartner, J., 1996. Estimate of the complete stress tensor to 8 km depth in the KTB scientific drill holes: implications for crustal strength, *J. geophys. Res.,* **102,** 18 453–18 475.

Burov, E.B. & Diament, M., 1995. The effective elastic thickness (T_e) of continental lithosphere: what does it really mean?, *J. geophys. Res.,* **100,** 3905–3927.

Byerlee, J., 1978. Friction of rocks, *Pure Appl. Geophys.,* **116,** 615–626.

Chapple, W.M., 1978. Mechanics of thin-skinned fold-and-thrust belts. *Geol. Soc. Am. Bull.,* **89,** 1189–1198.

Colman-Sadd, S., 1978. Fold development in Zagros simply folded belt, Southwest Iran, *AAPG Bull.,* **62,** 984–1003.

Comby, O., Lambert, C. & Coajou, A., 1977. An approach to the structural studies of the Zagros Fold Belt in the EGOCO Agreement Area, in *Proceedings of the Second Geological Symposium of Iran*, Tehran, pp. 103–159.

Costa, E. & Vendeville, B.C., 2002. Experimental insights on the geometry and kinematics of fold-and-thrust belts above weak, viscous evaporitic décollement, *J. Struct. Geol.,* **24,** 1729–1739.

Cotton, J.T. & Koyi, H.A., 2000. Modeling of thrust fronts above ductile and frictional detachments; application to structures in the Salt Range and Potwar Plateau, Pakistan, *Geol. Soc. Am. Bull.,* **112,** 351–363.

Dahlen, F.A., 1984. Noncohesive critical coulomb wegdes: an exact solution. *J. geophys. Res.,* **89**(B12), 10 125–10 133.

Dahlen, F.A., 1990. Critical taper model of fold-and-thrust belts and accretionary wedges, *Ann. Rev. Earth and Planet. Sci.,* **18,** 55–99.

Dahlen, F.A., Suppe, J. & Davis, D., 1984. Mechanics of fold-and-thrust belts and accretionary wedges: cohesive coulomb theory, *J. geophys. Res.,* **89**(B12), 10 087–10 101.

Davis, D., Suppe, J. & Dahlen, F.A., 1983. Mechanics of fold-and-thrust belts and accretionary wedges, *J. geophys. Res.,* **88**(B2), 1153–1172.

Davis, D.M. & Engelder, T., 1985. Role of salt in fold-and-thrust belts, *Tectonophysics,* **119,** 67–88.

De Mets, C., Gordon, R.G., Argus, D.F. & Stein, S., 1994. Effects of recent revision to the geomagnetic reversal time scale on estimates of current plate motions, *Geophys. Res. Lett.,* **21,** 2191–2194.

Déverchère, J., Petit, C., Gileva, N., Radziminovitch, N., Melnikova, V. & San'kov, V., 2001. Depth distribution of earthquakes in the Baikal rift system and its implications for the rheology of the lithosphere, *Geophys. J. Int.,* **146,** 1–26.

Egdell, H.S., 1996. Salt tectonism in the Persian Gulf Basin, in *Salt Tectonics*, Vol. 100, pp. 129–151, eds Alsop, G.I., Blundell., D.J. & Davison, I., Geological Society Special Publication, London.

Falcon, N., 1974. Zagros mountains, Mesozoic-Cenozoic orogenic belts (edited by Spencer, A.), *Spec. Pub. Geol. Soc. London* **4,** 199–211.

Ford, M., 2004. Depositional wedge tops: interaction between low basal friction external orogenic wedges and flexural foreland basins, *Basin Res.,* **16**(3), 361–375.

Goetze, C., 1978. The mechanics of creep in Olivine, *Phil. Trans. R. Soc. London,* **288,** 99–119.

Gutscher, M.A., Kukowski, N., Malavieille, J. & Lallemand, S., 1998. Material transfer in accretionary wedges from analysis of a systematic series of analog experiments, *J. Struct. Geol.,* **20**(407–416).

Hansen, F.D. & Carter, N.L., 1982. Creep of selected crustal rocks at 1000 MPa, *EOS, Trans. Am. geophys. Un.,* **63,** 437.

Hatzfeld, D., Tatar, M., Priestley, K. & Ghafori-Ashtiany, M., 2003. Seismological constraints on the crustal structure beneath the Zagros Mountain Belt (Iran), *Geophys. J. Int.,* **155,** 403–410.

Hessami, K., Koyi, H.A., Talbot, C.J., Tabasi, H. & Shabanian, E., 2001. Progressive unconformities within an evolving foreland fold-thrust belt, Zagros Mountains, *J. Geol. Soc.,* **158,** 969–981.

Homke, S., Verges, J., Garces, G., Emamia, H. & Karpuzc, R., 2004. Magnetostratigraphy of Miocene-Pliocene Zagros foreland deposits in the front of the Push-e Kush Arc (Lurestan Province, Iran), *Earth planet. Sci. Lett.,* **225,** 397–410.

Jackson, J., Haines, J. & Holt, W., 1995. The accomodation of Arabia-Eurasia plate convergence in Iran, *J. geophys. Res.,* **100**(B8), 15 205–15 219.

Jackson, J.A., 1980. Reactivation of basement faults and crustal shortening in orogenic belts, *Nature,* **283,** 343–346.

Jackson, J.A. & McKenzie, D., 1988. The relationship between plate motions and seismic moments tensors and the rates of active deformation in the Mediterranean and Middle East, *Geophys. J. Int.,* **83,** 45–73.

Jackson, M.P.A., Cornelius, R.R., Craig, C.H., Gansser, A., Stöcklin, J. & Talbot, C.J., 1990, *Salt diapirs of the Great Kavir, Central Iran,* in *Geological Society of America Memoir 177,* The Geological Society of America, Boulder, CO, USA.

Jaeger, J. & Cook, N.G.W., 1979, *Fundamental of Rock Mechanics*, 3rd edn, Chapman & Hall, London, p. 593.

Jaumé, S.C. & Lillie, R.J., 1988. Mechanics of the Salt Range-Potwar Plateau, Pakistan: a fold-and-thrust belt underlain by evaporites, *Tectonics,* **7**(1), 57–71.

Kukowski, N., Lallemand, S.E., Malavieille, J., Gutscher, M.A. & Reston, T.J., 2002. Mechanical decoupling and basal duplex formation observed in sandbox experiments with application to the Western Mediterranean Ridge accretionary complex, *Mar. Geol.,* **186,** 29–42.

Lacombe, O. & Mouthereau, F., 2002. Basement-involved shortening and deep detachment tectonics in forelands of orogens: insights from recent collision belts (Taiwan, Western Alps, Pyrenees), *Tectonics,* **21**(4), doi:10.1029/2001TC901018.

Maggi, A., Jackson, J.A., Priestley, K. & Baker, C., 2000. A re-assessment of focal depth distributions in southern Iran, the Tien Shan and northern India: do earthquakes really occur in the continental mantle ? *Geophys. J. Int.,* **143,** 629–661.

Meigs, A.J. & Burbank, D.W., 1997. Growth of the South Pyrenean orogenic wedge, *Tectonics,* **16**(2), 239–258.

McQuarrie, N., 2004. Crustal scale geometry of the Zagros fold-thrust belt, Iran, *J. Struct. Geol.,* **26,** 519–535.

Molinaro, M., Guezou, J.C., Leturmy, P., Eshraghi, S.A. & Frizon de Lamotte, D., 2004. The origin of changes in structural style across the Bandar Abbas syntaxis, SE Zagros (Iran), *Mar. Petrol. Geol.,* **21,** 735–752.

Molinaro, M., Leturmy, P., Guezou, J.-C., Frizon de Lamotte, D. & Eshraghi, S.A., 2005. The structure and kinematics of the south-eastern Zagros fold-thrust belt; Iran: from thin-skinned to thick-skinned tectonics. *Tectonics,* **24,** doi:10.1029/2004TC001633.

Motiei, H., 1993. *Geology of Iran : Stratigraphy of Zagros*, Geological Survey of Iran.

Mouthereau, F. & Petit, C., 2003. Rheology and strength of the Eurasian continental lithosphere in the foreland of the Taiwan collision belt: constraints from seismicity, flexure and structural styles, *J. geophys. Res.,* **108**(B11), 2512, doi:10.1029/2002JB002098.

Ni, J. & Barazangi, M., 1986. Seismotectonics of the Zagros continental collision zone and a comparison with the Himilayas, *J. geophys. Res.,* **91**(B8), 8205–8218.

O'Brien, C.A.E., 1957. Salt diapirism in South Persia, *Geologie en Mijnbouw*, 337–376.

Roobol, M.J., Ramsay, C.R., Jackson, N.J. & Darbyshire, D.P.F., 1983. Late Proterozoic lavas of the Central Arabian Shield-evolution of an ancient volcanic arc system, *J. Struct. Geol.,* **140**(2), 185–202.

Sepher, M. & Cosgrove, J.W., 2004. Structural framework of the Zagros Fold-Thrust Belt, Iran, *Mar. Petrol. Geol.,* **21,** 829–843.

Sherkati, S., 2004. Style tectonique et cinématique du plissement dans le Zagros Iranien (zone d'Izeh) : conséquences pétrolières. In: *IFP*. Université Cergy-Pontoise, Rueil-Malmaison, p. 224.

Sherkati, S. & Letouzey, J., 2004. Variation of structural style and basin evolution in the central Zagros (Izeh zone and Dezful Embayment), Iran, *Mar. Petrol. Geol.,* **21**(5), 535–554.

Smit, J.H.W., Brun, J.P. & Sokoutis, D., 2003. Deformation of brittle-ductile thrust wedges in experiments and nature, *J. geophys. Res.,* **108**(B10), 2480, doi:10.1029/2002JB002190.

Snyder, D.B. & Barazangi, M., 1986. Deep crustal structure and flexure of the Arabian plate beneath the Zagros collisional mountain belt as inferred from gravity observations, *Tectonics,* **5**(3), 361–373.

Stocklin, J., 1968. Structural history and tectonics of Iran; a review. *AAPG Bull.,* **52**(7), 1229–1258.

Stocklin, J., 1974. Possible ancient continental margins in Iran, in *Geology of continental margins*, pp. 873–877, eds Burk, C. & Drake, C., New York.

Talbot, C.J. & Alavi, M., 1996. The past of a future syntaxis across the Zagros, in Alsop, in *Salt Tectonics*, Vol. 100, pp. 89–109, eds Alsop, G.I., Blundell., D.J. & Davison, I., Geological Society of America Special Paper.

Talebian, M. & Jackson, J.A., 2004. A reappraisal of earthquake focal mechanisms and active shortening in the Zagros mountains of Iran, *Geophys. J. Int.,* **156,** 506–526.

Tatar, M., Hatzfeld, D. & Ghafori-Ashtiany, M., 2004. Tectonics of the Central Zagros (Iran) deduced from microearthquakes seismicity, *Geophys. J. Int.,* **156,** 255–266.

Toussaint, G., Burov, E. & Avouac, J.-P., 2004. Tectonic evolution of a continental collision zone: a thermomechanical numerical model, *Tectonics,* **23,** TC6003, doi:10.1029/2003TC001604.

Turcotte, D.L. & Schubert, G., 1982, *Geodynamics: Applications of Continuum Mechanics to Geological Problems*, Wiley, New York.

Vernant, P. *et al.*, 2004. Present-day crustal deformation and plate kinematics in the Middle East constrained by GPS measurements in Iran and northern Oman, *Geophys. J. Int.,* **157,** 381–398.

Weijermars, R., Jackson, J.A. & Vendeville, B., 1993. Rheological and tectonic modeling of salt provinces, *Tectonophysics,* **217,** 143–174.

Wessel, P. & Smith, W.H.F., 1998. New version of the Generic Mapping Tools released, *EOS, Trans. Am. geophys. Un.,* **79,** 579.

Wilks, K.R. & Carter, N.L., 1990. Rheology of some continental lower crust, *Tectonophysics,* **182,** 57–77.

Williams, C.A., Connors, C., Dahlen, F.A., Price, E.J. & Suppe, J., 1994. Effect of the brittle-ductile transition on the topography of compressive mountain belts on Earth and Venus, *J. geophys. Res.,* **99**(B10), 19 947–19 974.

Zoback, M.D. & Healy, J.H., 1992. In situ stress measurements to 3.5 km depth in the Cajon Pass scientific research borehole: implications fore mechanics of crustal faulting, *J. geophys. Res.,* **97,** 5039–5058.